Thermal management during direct laser deposition (DLD) of Ti-6Al-4V components

by

Katie McDonald

A thesis submitted to
School of Engineering
University of Birmingham
for the degree of
MASTER OF RESEARCH

Department of Metallurgy and Materials
School of Engineering
University of Birmingham
July 2013

Acknowledgements

I would like to take this opportunity to thank the University of Birmingham, BAE Systems and the Engineering and Physical Science Research Council (EPSRC) for the funding and equipment they provided for this project.

I would also like to thank Moataz Attallah and Mark Ward for their supervision, encouragement and advice throughout the project. Thanks also to Andy Wescott, Eirian Hughes and Ravi Aswathanarayanaswamy for the technical support, time, many explanations and very useful chats.

Finally, thank you to my family and to David Fishpool, for their constant support.

Abstract

Direct Laser Deposition (DLD) introduces steep thermal gradients into components due to the localised, high temperature melt region created by the laser heat source. This causes local thermal expansion and plastic deformation during heating and leads to a permanent change in the geometry of the component, which may mean it is no longer fit for purpose. There is also an effect on the microstructure and therefore mechanical properties.

Understanding the relationship between residual stresses, microstructural development and thermal cycling during DLD will mean that distortion and microstructure can be predicted by understanding the thermal profile of a DLD repair. The process can then be optimised to attain the desired microstructure and to control or reduce distortion.

In this study, temperature measurements were taken across a substrate during DLD repair, under varying controlled thermal conditions (heated substrate, cooled substrate, insulated substrate, clamped and unclamped substrate). This data was used to calculate the cooling rates at different locations, and these were correlated to the observed distortion of the substrate and changes in microstructure. The porosity of the deposited material and the size of the heat affected zone improved inversely to one another with regard to the thermal conditions. This is not because a small heat affected zone causes low porosity or vice versa, it is because in the case of Ti-6Al-4V the same processing conditions are needed to produce both effects.

The cooling rates were calculated using thermocouple readings from across the substrate over time after processing, and the corresponding microstructure was characterised using metallurgical analysis. It was found that cooling rate varied significantly at the outer edges of

the substrate but hardly at all near the processing area, indicating that while the thermal gradient across the plate will affect distortion, it has little effect on microstructure.

The distortion was measured by using 3D laser scanning to compare the geometry of each substrate before and after processing. When the measured distortion was plotted against the cooling rate in the same location, there was evidence of an inverse binomial form relationship. Despite the relatively small size of the study this is an indicator of how the DLD process can be developed further.

Contents

List of Figures

List of Tables

1. Introduction

1.1 Scope of project

The emphasis of this research project is to study issues associated with using direct laser deposition to repair worn, damaged or poorly manufactured components and to characterise the repair quality. Repair applications are of interest to many industries because of the drive for greater sustainability in manufacturing.

A number of additive manufacturing processes have been developed in parallel at different establishments, but they all involve the supply of metallic materials, either powder or wire, into a laser- or electron beam-generated heat spot where the material is melted and forms a melt pool which quickly solidifies into metal layers. Parts are built to completion layer by layer from bottom to top. The research work in this thesis was carried out at the Advanced Technology Centre, Filton, using a coaxial powder feed and a three axis Nd:YAG laser source. This is commonly known as direct laser deposition or DLD.

DLD presents an opportunity to extend the lifetime of damaged components, reducing the cost of replacements and potentially the time a component is out of action. The advantages of DLD over conventional repair techniques include the relatively localised heat input required which leads to less distortion and a smaller heat affected zone. It is also possible to carry out *in situ* repairs and the precise deposition creates a near net shape that requires minimal finishing processes.

DLD is an important process in the aerospace industry that has potential for making a far reaching difference in manufacturing and through-life management of platforms. Its key attributes are that it is a purely additive process and thus makes very efficient use of

material, and that the process is flexible with components made directly from CAD files with little hard tooling [1].

One of the major applications for Ti-6Al-4V is in manufacturing aircraft structural parts where it has advantages over competing metallic and composite materials such as higher yield stress and fatigue strength, better corrosion resistance and high modulus of elasticity. For example, forged Ti-6Al-4V with fully lamellar microstructure has been used for landing gear on the Boeing 747 aircraft and the bulkhead for a twin engine military aircraft due to its good fatigue crack growth resistance [2].

Broader investigation of using DLD technology for repairing Ti-6Al-4V, Ti-6242 and Ti-17 alloys, which are used in high pressure turbines and aeronautical engines, has been carried out [3]. The aim of this was to create a chain of laser applications that prevent wastage of damaged components that may be repairable. Successful process parameters were presented as well as suggestions for future direct laser deposition of entire blades.

The key to the uptake of this technology, particularly in the aerospace industry, is the mechanical and metallurgical properties of the fabricated components. These are largely dependent on the thermal cycle that the component undergoes during processing. In order to control and modify the microstructure and so make the DLD parts fit for purpose, a good understanding of the temperature cycles and influence on the metallurgy of the parts is required.

1.2 Aims and objectives

The aim of this project is to assess by experimentation the influence of thermal boundary conditions on the thermal cycles, microstructure and distortion of Ti-6Al-4V repairs performed by DLD.

The objectives are to understand the influence of thermal boundary conditions on the thermal cycling, microstructure and distortion and to use analytical models to describe the process parameters such as laser operating parameters and thermal material properties. Thermocouple measurements taken experimentally will be used to calibrate images taken using a thermal imaging camera and to validate assumptions about the thermal cycle that the substrates will undergo during DLD.

The project also aims at developing an understanding of the relationship between cooling rate and distortion, and to use the collected data to quantify this relationship. The thermocouples can be used to identify locations where the temperature has been monitored over the entire processing time so that maximum cooling rates can be found and compared with the distortion which that part of the plate has undergone.

The influence of thermal boundary conditions on the resulting DLD repairs and the relationship between cooling rate and distortion in Ti-6Al-4V plates is necessary information in the development of the DLD process for industrial use. As the understanding of these relationships improves, the process can be more easily optimised.

2 Literature review

Grade 5 Titanium alloy (Ti-6Al-4V) has been of interest to the aerospace industry for several decades because of its material properties. Direct laser deposition now offers the chance to produce components from this versatile alloy in a sustainable, cost-efficient way. DLD has been used with a number of other materials, mainly 316L stainless steel and this has developed an understanding of the process. However, some properties of Ti-6Al-4V make it a more challenging alloy to work with than other common aerospace materials. The main reason for this is its low thermal diffusivity, which means that steep thermal gradients can develop in components being made by DLD.

2.1 Ti-6Al-4V

Titanium is one of the most commonly used aerospace alloys due to its high strength-to-weight ratio and excellent corrosion resistance. It is also an expensive material as the process used for extracting titanium, the Kroll process, is resource-intensive and its high chemical reactivity places strict requirements on the manufacturing steps. Working with Ti-6Al-4V can be inefficient due to difficulties with traditional manufacturing processes, where a machining error or other damage often leads to the component being abandoned as scrap [4]. The relative scarcity and cost of titanium makes this approach cost-prohibitive and so significant effort is therefore being given to developing new production routes and manufacturing technologies to allow wider use of titanium.

Ti-6Al-4V is the most commonly used α+β titanium alloy. As well as aircraft components, it is used at temperatures up to 400°C in chemical processing equipment, surgical implants, marine hardware and automotive applications [5].

2.1.1 Physical metallurgy

Titanium is an allotropic element, meaning it can occur and is stable in more than one crystal state. It has two primary crystallographic phases, an α-phase hexagonal close packed structure (HCP) and a β-phase body centred cubic structure (BCC) [4]. The size, shape and relative distribution of these two phases are key factors in determining the microstructure of the titanium and its subsequent mechanical properties.

Titanium alloys can be classified into three major categories according to the predominant phases present in the microstructure: α alloys, β alloys and α+β alloys. Fundamental to controlling the formation of the α-phase and the β-phase is the β transus temperature, which is the temperature at which the β-phase reverts to an α-phase [6]. This transus temperature varies with alloy composition, but all titanium alloy processing must take the transus temperature into account in order to produce the desired microstructure.

The α alloys have relatively high strengths, high oxidation resistance and the best weldability of the titanium alloys, but they are more difficult to form than β alloys. β alloys have good hardenability, good cold formability when they are solution treated and high strength when they are aged. β alloys are slightly denser than other titanium alloys and the least creep resistant, but they are weldable and can have high yield strengths of up to 1345 MPa [2]. This compares favourably with other common structural materials (see Table 1).

Material	Yield Strength (MPa)
ASTM A36 steel	250
Aluminium alloy	400
Stainless steel	520

Table 1. Typical yield strength of common structural materials [5]

α+β alloys are heat treatable and most of them are weldable. They have relatively high strength but the high temperature creep strength is not as good as most α alloys. The cold forming of α+β alloys is limited but hot forming qualities are quite good and many can be superplastically formed [4]. Ti-6Al-4V is one of the most commonly used commercial titanium alloys because of its high strength and high fatigue resistance.

2.1.2 Microstructure and phase transformations

The elements that are included in the manufacture of titanium alloys may encourage the stabilisation of either the α or the β phase (see Figure 1). Ti-6Al-4V contains both an α stabiliser and a β stabiliser so it can be strengthened by heat treatment or by thermo-mechanical processing. Oxygen is also an important α stabiliser and so if it is introduced into the alloy during processing it will strengthen the alloy but may also cause embrittlement.

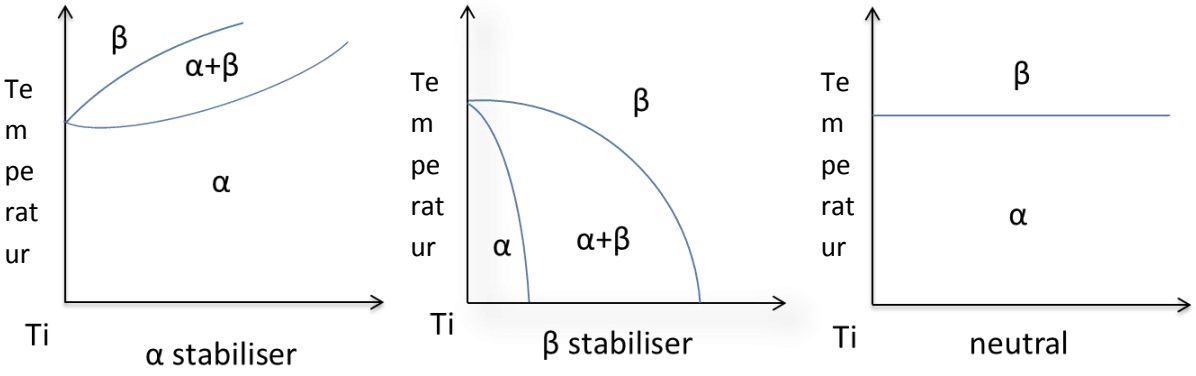

Figure 1. Effect of alloying elements on phase diagram of titanium alloys (schematically) [4]

The transus temperature of Ti-6Al-4V is influenced by both the α and the β stabilisers and is 980°C ± 15°C [4].

The typical microstructure of Ti-6Al-4V can be classified into three different categories: lamellar, equiaxed or bimodal (see Figure 2). The relationship between DLD processing parameters and microstructures in as-deposited Ti-6Al-4V, and an understanding of microstructure evolution is critical for both process control and process design because microstructure plays an essential role in controlling mechanical properties [7]. The microstructure of Ti-6Al-4V has been extensively studied and it has been observed by many different groups that its development is highly dependent upon maximum temperature and cooling rate [8,9,10].

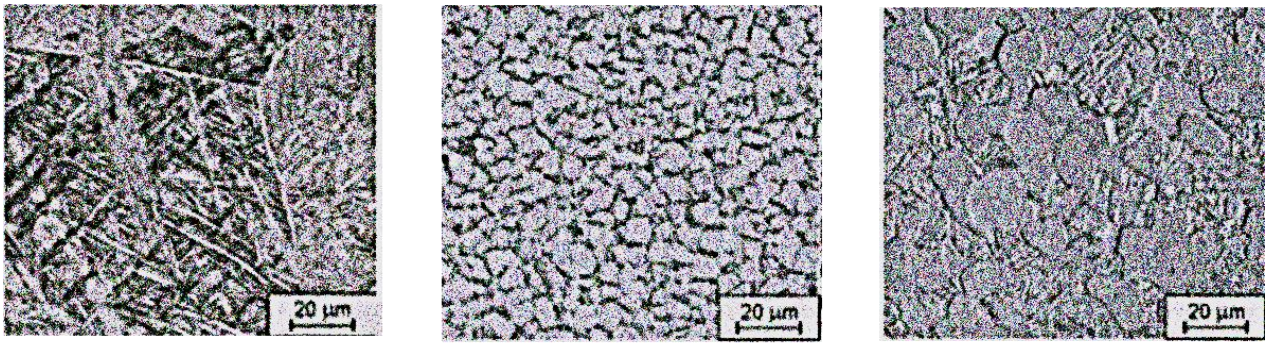

Figure 2. Micrographs showing Ti-6Al-4V with typical (a) lamellar, (b) equiaxed and (c) bimodal microstructure [11]

The lamellar structures can be controlled by heat treatment [12]. Furnace (slow) cooling from above to below the β transus temperature leads to nucleation and growth of the α phase in plates, starting from the β grain boundaries. The resulting lamellar microstructure is fairly coarse and known as plate-like α. Air (fast) cooling results in a fine, needle-like α phase known as acicular α (see Figure 3).

A Widmanstätten structure is developed by intermediate cooling rates. α-Widmanstätten plate size increases when the cooling rate decreases and tensile strength is reduced by about 80 MPa. Water quenching from the β-phase field temperature followed by annealing in the α+β phase region leads to a much finer lamellar structure, alpha prime (α'), also called martensite [8].

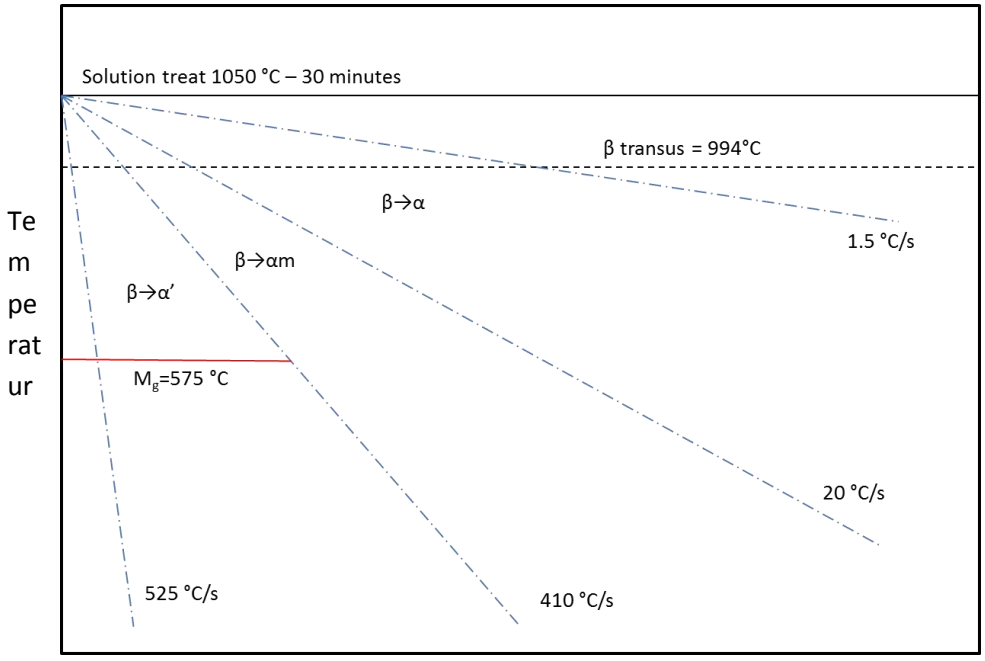

Figure 3. Schematic continuous cooling diagram for Ti-6Al-4V treated at 1050°C for 30 minutes [13]

Martensitic microstructures are rarely present in structural components as they only form at very high cooling rates, but they can occur when using laser processing methods. The martensitic microstructures can be transformed to a fine lamellar α+β structure by annealing in the temperature range 700°C-850°C. The β phase is formed as a continuous layer between the martensitic plates [4].

The equiaxed structures are obtained by extensive mechanical working on the material in the α+β region, where the lamellar structure is broken up into equiaxed α. Subsequent annealing at about 700°C produces the mill-annealed structure. The bimodal structure consists of isolated primary α grains in a transformed β matrix. This structure can be

obtained by annealing at 955°C for one hour followed by water quenching, or by air cooling and aging at 600°C [4].

2.1.3 Mechanical properties

Variations in the microstructure of Ti-6Al-4V lead to different material properties and the qualitative correlation between microstructural parameters and the mechanical properties are summarised in Table 2. For example, it explains that microstructural features such as secondary α particles in the β phase can increase the yield strength of the material but cause a decrease in ultimate tensile strength.

	Yield stress $\sigma_{0.2}$	UTS ε_F	High cycle fatigue	Micro-cracks ΔK_{th}	Creep strength
Small α colonies, α lamellae[a]	+	+	+	+	+/-
Bi-modal structure[b]	+	+	-	+	-
Small α grain size[c]	+	+	+	+	-
Aging (α_2), oxygen	+	-	+	-	+
Secondary α in β	+	-	+	+	+

[a] Compared to coarse lamellar structure

[b] Compared to fully lamellar structure with same cooling rate

[c] Compared to large α grain size of fully equiaxed structures

Table 2. Qualitative correlation between microstructure and mechanical properties of Ti-6Al-4V [4]

The difference in mechanical properties of water quenched, air cooled and furnace cooled Ti-6Al-4V have been investigated and it has been found that in general the hardness increases with the increase of annealing temperature, reaching saturation at 1050°C. For material quenched from the same temperature, hardness decreases with the decrease of the cooling rates. The tensile strength of Ti-6Al-4V behaves in the same manner as hardness, increasing with the increase of cooling rates and annealing temperature (see Table 3).

	Temperature	$\sigma_{0.2}$	UTS	σ_F	Elasticity	Reduction in area
	°C	MPa	MPa	MPa	%	%
Lamellar	Room temp	925	1015	1145	5	12
Bi-modal (20% vol α')	Room temp	995	1100	1350	13	20
Bi-modal (30% vol α')	Room temp	955	1060	1365	13	26
Lamellar	600	515	640	800	10	26
Bi-modal (10% vol α')	600	570	695	885	10	30
Bi-modal (40% vol α')	600	565	670	910	14	36

Table 3. Tensile properties of the α+β titanium alloy IMI 834 [20]

The size of α grains in a fully equiaxed microstructure corresponds with high cycle fatigue strength. As the size of the α grains decreases the high cycle fatigue strength increases. Tensile ductility is generally very high and increases as grain size decreases [4]. The feasibility of obtaining a specific microstructure has to be considered for commercial applications. For example, the high fatigue strength of a small grained microstructure is difficult to obtain in a

fully lamellar microstructure as the required cooling rate would be more than 1000°C/min, which can only be obtained in thin sections. In bi-modal microstructures the temperature region needed to obtain the small grain sizes is too high to be commercially viable.

2.2 Direct laser deposition

In direct laser deposition (DLD), powder is fed continuously into a molten pool on the surface of the substrate or previously deposited layer (see Figure 4). The molten pool is generated and maintained through an interaction with the laser beam and the powder injected into the pool forms another deposited layer after solidification. The substrate or deposited layer is melted to obtain good metallurgical bonding between the substrate and deposited layer or between successive deposited layers, in most cases to the depth of approximately one millimetre [14].

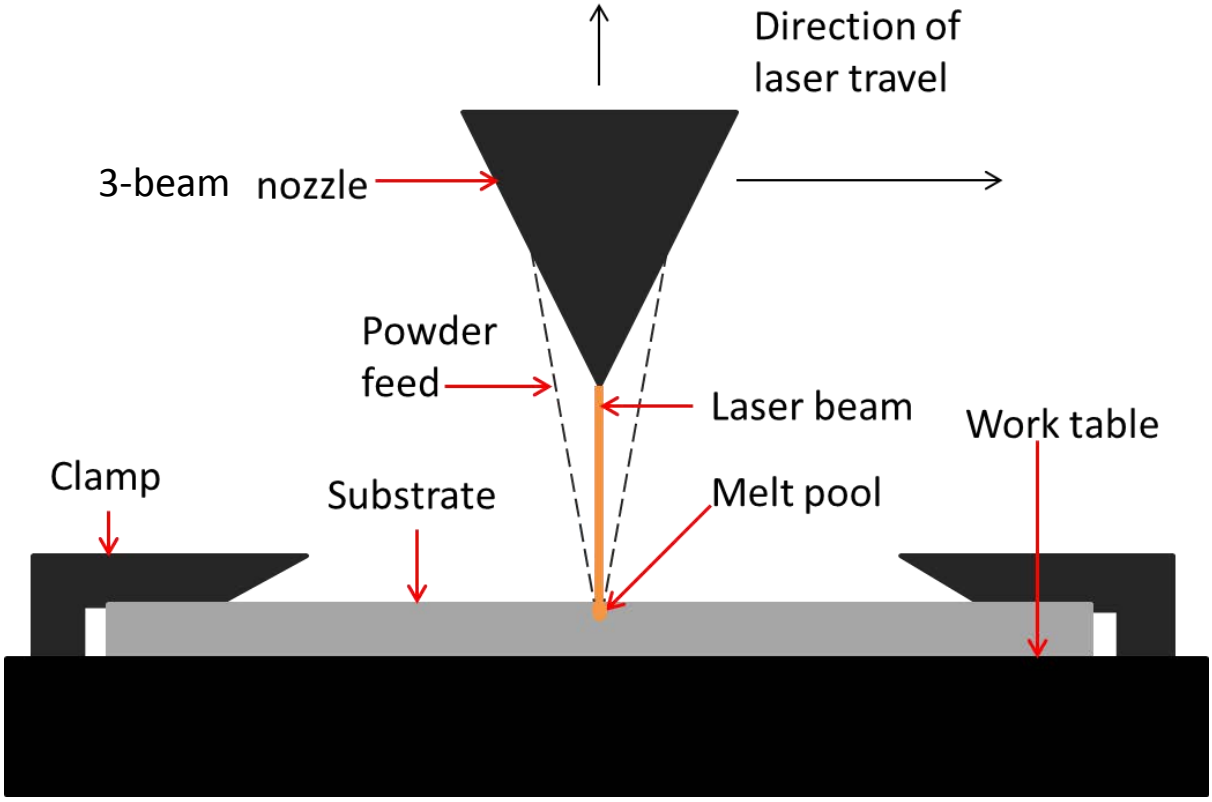

Figure 4. Schematic diagram of the DLD process

Good powder consolidation is achieved by controlling the energy input at every location during the build. Energy input is a function of laser power, laser scanning speed and powder feed rate [15].

Direct laser deposition can be used for producing new components, adding features to existing components, hybrid manufacturing or for repairing damage. It is possible to produce geometries that would not be possible using a single manufacturing process otherwise and therefore reduces the need for joins, which are often the weak point in a component. When adding secondary features to an existing component, DLD has the advantage of causing only a limited heat affected zone due to the small width of the laser melt pool.

In the last decade, much work has been done to characterise the microstructure of direct laser fabricated Ti-6Al-4V and to understand the effect of the process variables on the quality of builds. Initially each process variable was considered individually and extensive parameter optimisation was undertaken by a number of groups, but more recently the focus of research has been on how combinations of parameters influence the thermal profile and history of each component.

2.2.1 Comparison of DLD with alternative additive manufacturing processes

Among additive manufacturing layer technologies, the processes can be largely divided into laser metal deposition (LMD) processes and selective laser melting (SLM) processes. The most important difference between these is the provision of the powder material. In laser metal deposition processes, the powder is supplied by a powder feeding nozzle, while for selective laser melting the part is fabricated in a “powder bed”. In both processes the powder is completely melted by the laser beam, resulting in the fully dense layers [3].

Powder bed manufacturing involves the use of a high power laser to fuse small particles of plastic, metal, ceramic, or glass powders into a solid three-dimensional shape. The laser selectively melts powdered material by scanning cross-sections that are generated from a CAD file on the surface of a powder bed. After each cross-section is scanned, the powder bed is lowered by one layer thickness, a new layer of material is applied on top, and the process is repeated until the part is completed (see figure 5).

Powder bed manufacturing typically uses a pulsed laser as the finished part density depends on peak laser power, rather than laser duration The bulk powder material in the powder bed is preheated to just below its melting point, to make it easier for the laser to raise the temperature of the selected regions the rest of the way to the melting point

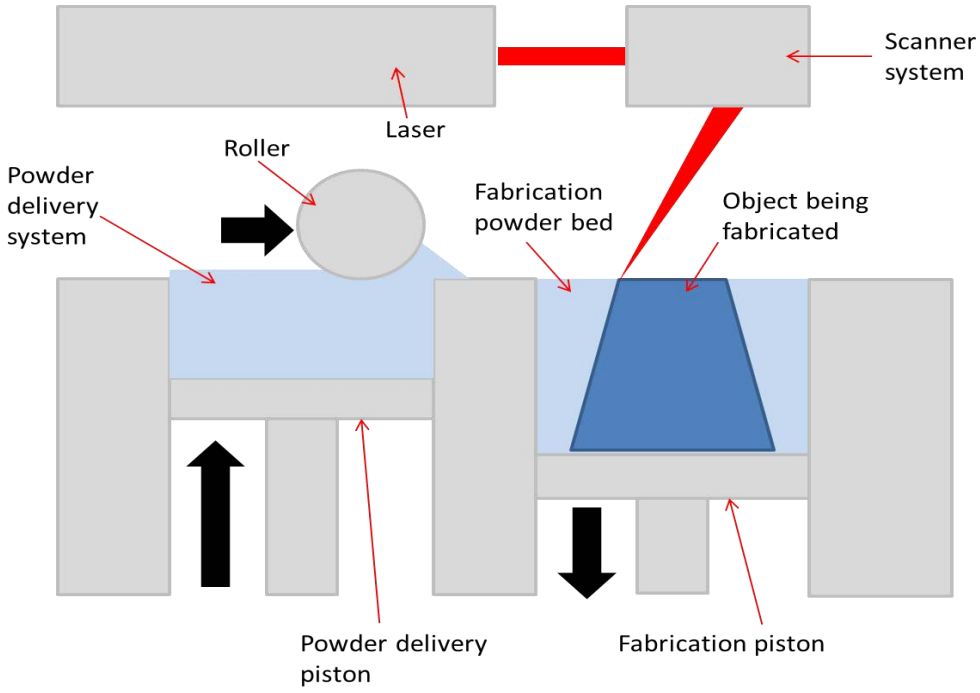

Figure 5. Schematic diagram of powder bed manufacturing process

Unlike some other additive manufacturing processes, powder bed manufacturing does not require support structures as the part being constructed is surrounded by unmelted powder at all times, allowing for the construction of previously impossible geometries.

Compared with direct laser deposition, powder bed manufacturing can produce parts from a relatively wide range of commercially available powder materials and the physical process can be full melting, partial melting, or liquid-phase sintering. Depending on the material, up to 100% density can be achieved with material properties comparable to those from conventional manufacturing methods. In many cases large numbers of parts can be packed within the powder bed, allowing very high productivity [12].

The precision and geometrical freedom of powder bed processing is higher than that of DLD, however it does not provide the ability to build-up material layers directly on three dimensional surfaces and to process of very large parts that are the main advantages of DLD and enable the use of DLD for repair and wear/corrosion protection applications [3].

2.2.2 Development of the process

Lasers have provided industry with a controllable and highly directional heat source since they were invented in the 1950s. Since then, laser beams have been widely used in many manufacturing industries performing tasks such as cutting, welding, surface heating, bending, melting, alloying, cladding, texturing, roughening, marking and cleaning.

A new application in the field of rapid prototyping emerged in the 1980s, using lasers to produce functional and net shape or near net shape components with a desired geometry in a single step. As well as significant advantages over conventional processes, there is also

very little material waste since there is only a small amount of post-deposition machining required and most of the unused powder can be recycled without contamination [16].

A typical development procedure for producing a component by DLD involves writing a motion path for the laser beam during the build and the optimisation of processing parameters to achieve a fully dense part with a desirable microstructure at the maximum operating speed. A large number of operating parameters and physical phenomena determine the quality of the fabricated part and several of these are concerned with the resulting geometry. Figure 6 shows the typical cross section of a laser welding bead, where *h* is the bead height, *w* is the bead width, *Θ* is the angle of wetting and *b* is the fusion depth representing the thickness of substrate melted during the laser processing. The fusion depth determines the depth of the dilution of one layer into another [17].

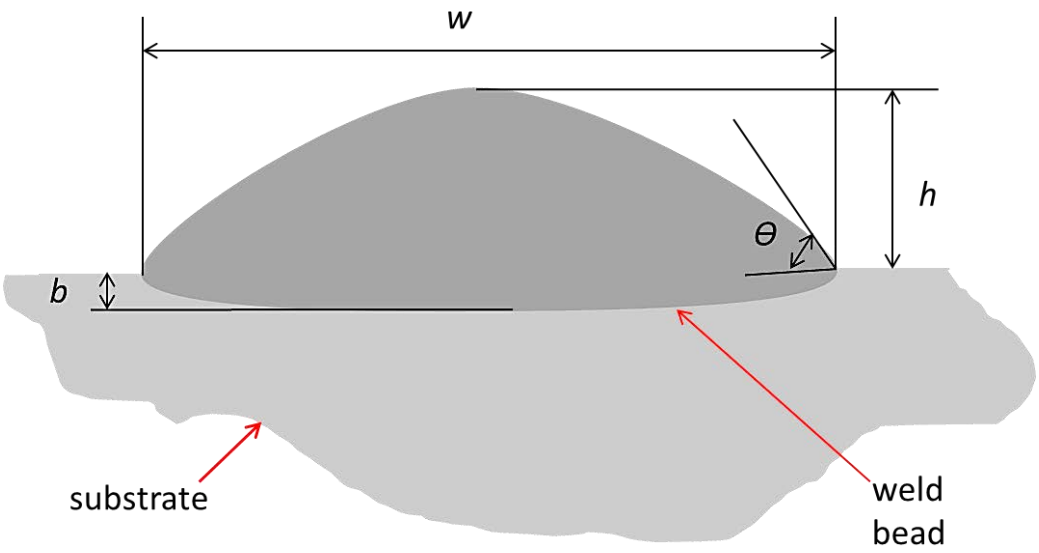

Figure 6. Typical cross section of a laser weld bead [16]

2.2.3 Process variables

As the parameters control the thermal cycles and therefore fusion between layers, homogeneity of the layers, surface finish, porosity and cracking due to thermal stresses, it is often necessary to perform several iterations in order to optimise the parameters.

It is currently possible to produce near fully dense components close to net shape and so the next requirement is microstructural control. The effect of laser power on the microstructure of grade 316 stainless steel has been examined in previous studies and it was found that cell structures which formed at lower powers (115-275 W) were finer than those formed at higher powers (345-410 W) [18]. The initial cooling rate of the molten pool formed at higher powers is faster than those formed at lower powers and the composition difference is seen to be more pronounced when the material is solidified slowly.

The detailed variation of morphology and grain size in DLD 316L stainless steel was investigated and it was found that a predominantly columnar and highly refined microstructure tended to form at the base of the component, near the substrate [19]. The grains became coarser in subsequent layers and a predominantly equiaxed structure was formed at the top of the component (see Figure 7). It was concluded that grain size and microstructure were dominated by the combination of the laser power and laser scanning speed but were largely independent of powder feed rate

In the study of titanium, a preliminary investigation examined varying process parameters and the effect on the microstructure of a burn resistant alloy Ti-25V-15Cr-2Al-0.2C (wt. %) [20]. It was found that this alloy generally formed equiaxed grains under most processing conditions and a few elongated columnar grains tended to form at the bottom the sample.

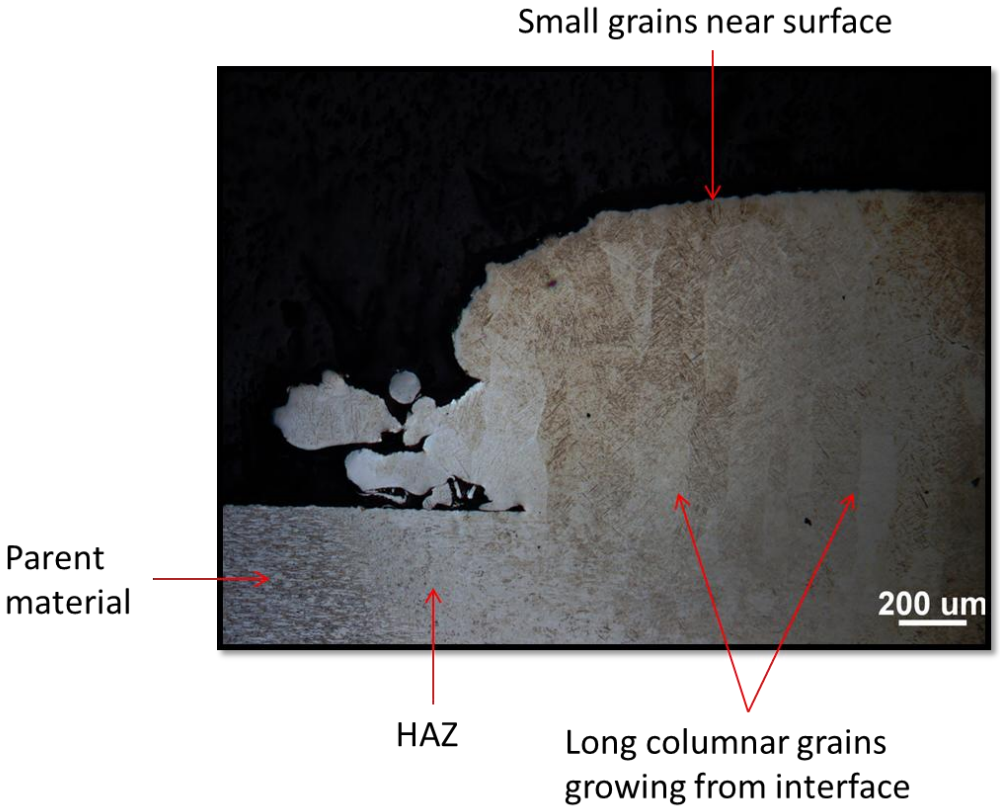

Figure 7. Micrograph showing the growth of columnar grains in Ti-6Al-4V during DLD

Studies using Ti-6Al-4V investigated the effect of laser power, laser scanning speed and powder feed rate on the variation in size of the columnar structure formed. It was found that the grain size tends to increase with the increase of laser power and the decrease of laser scanning speed, although the effect of each parameter was not linear [21,22,23]. Another study using Ti-6Al-4V samples also recognised that large columnar prior-β grains and layer bands are the characteristic morphology for DLD components [24]. It showed that columnar grains are able to grow through multiple deposited layers due to epitaxial growth from previously solidified layers. When loading is perpendicular to the grain growth direction this structure is undesirable as it has reduced tensile strength due to the increased presence of grain boundaries along the load path. Ti-6Al-4V is susceptible to the formation of

columnar grains during laser deposition because heat loss through the substrate initially leads to more rapid cooling via the substrate [10]. This causes directional growth counter to the cooling direction. As laser power increases, the columnar grains become shorter until they are replaced with large equiaxed grains. However, it has been shown that as temperature increases, the grain growth kinetics are faster and for a given temperature the grain size will increase with time [8].

At lower powers there is a change towards a very porous structure which is caused by incomplete melting of the powder [10]. At intermediate powers there is pin-hole porosity as the result of shrinkage during cooling.

Advances in stereology and microscopy permit rapid characterisation of various features in Ti alloys including Widmanstätten α-laths, grain sizes, grain shapes, colony structures and volume fractions of different phases [25]. The aim is to minimise human subjectivity to produce accurate and repeatable results.

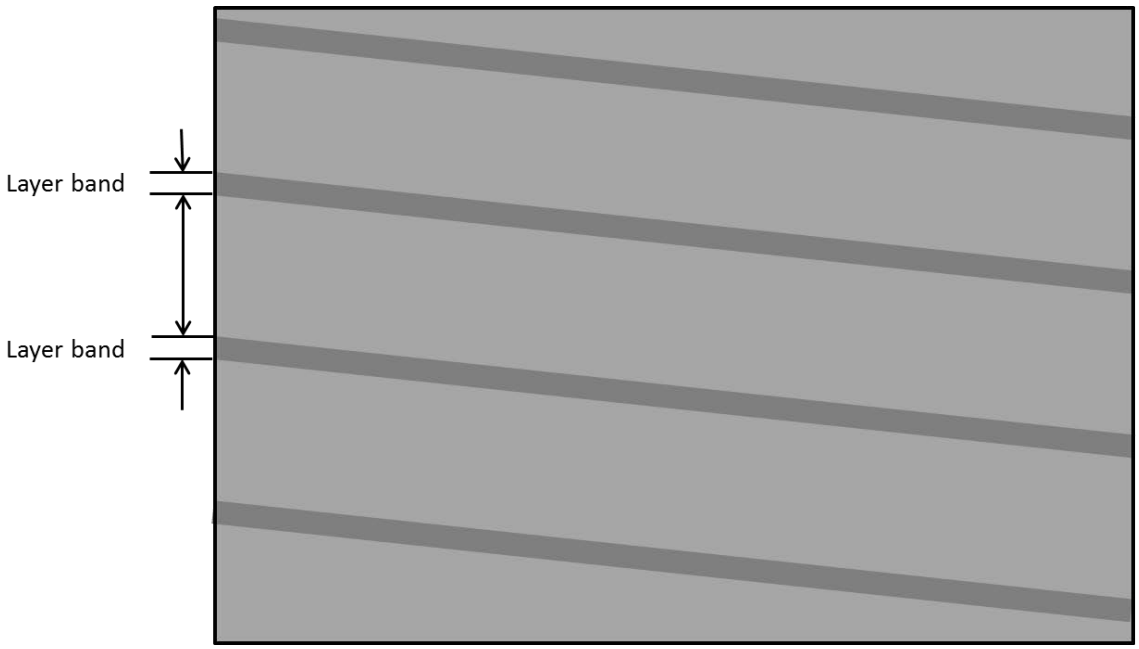

Figure 8: Diagram showing layer bands caused by microsegregation in titanium alloy [26]

The layer bands are a result of micro-segregation in the solidifying melt pool and the complex thermal history that the part undergoes as each layer is built (see Figure 8). The microstructure of the layer band consists of large colonies of acicular α outlined in transformed β, whereas the adjacent material consists of smaller colonies with the same type of structure [24].

2.3 Thermal effects due to DLD

Thermal radiation is the electromagnetic radiation generated by the thermal motion of charged particles in all matter with a temperature greater than absolute zero. The effect of temperature changes that take place during direct laser deposition of components is key to understanding and predicting the final microstructure.

2.3.1 Measurement

Infra red (IR) covers a portion of the electromagnetic spectrum from approximately 0.9-1000 micrometers and is not detectable by the human eye. The intensity of the emitted energy from an object varies with temperature and radiation wavelength. In addition to emitting energy from an object, an object reacts to incident radiation from its surroundings by absorbing and reflecting a portion of it [27].

A thermal imaging camera can convert it to a digital image which shows thermal variation across an object, allowing non-contact measurements of an object's temperature. This is useful in direct laser deposition due to the difficulty of locating thermocouples in a moving melt pool. Other wavelengths could be used, for example those in the "visible" range, but the IR range is less affected by background lighting. At temperatures below 500°C there is much more infra-red emission than visible emission.

Thermocouples can be used for measuring the change in temperature across a substrate, moving away from the applied heat source. The change in temperature over time and distance is central to describing the thermal history of a component which has been made or repaired using DLD.

2.3.1.1 Emissivity corrections

The radiative properties of the objects are usually described in relation to a perfect blackbody. If the emitted energy from a blackbody is denoted as W_{bb} and that of the object at the same temperature as W_{obj}, then the ratio between these two values describes the emissivity ε of the object;

$$\varepsilon = W_{obj}/W_{bb} \qquad \text{Equation 1}$$

Emissivity is a number between 0 and 1. The better the radiative properties of the object, the higher the emissivity value.

An infra-red camera calculates temperature based on radiance measurements and the emissivity of the object. In most applications the emissivity is based on standard values from a table but when it is unknown or uncertain, it can be calculated by reversing the process. If the temperature is known then emissivity can be calculated.

The simplest method of establishing emissivity is the “adjacent spot” method [27]. The temperature of an object is determined using an area of known emissivity. The object is then adjusted so that the area with known emissivity is close enough to an area with unknown emissivity that the two areas can reasonably be assumed to have the same temperature. Using this temperature the unknown emissivity value can be calculated.

2.3.2 Thermal history

The correlation between microstructure and processing parameters is not straightforward and it is not easy to isolate the effect of altering individual parameters on the final microstructure of a DLD component. However, the microstructure is strongly influenced by the thermal history which the component has undergone and thermal history can be

measured, predicted and controlled in a much simpler way than attempting to directly control the microstructure. A large amount of work has already been carried out to understand and control the thermal cycles during DLD of components [19,28,29].

The thermal profile created by DLD differs depending on the processing parameters, component geometry and thermal boundary conditions. In order to control the microstructure and mechanical properties there must be an understanding of the relationship between thermal profile and microstructural evolution, and how the thermal profile can be managed.

2.3.2.1 Development of thermal gradients in DLD

The thermal gradient is the physical quantity that describes the direction and rate of temperature change around a particular location. In the DLD process the energy source is the laser, which hits the substrate at an angle a with respect to the surface normal (see Figure 9).

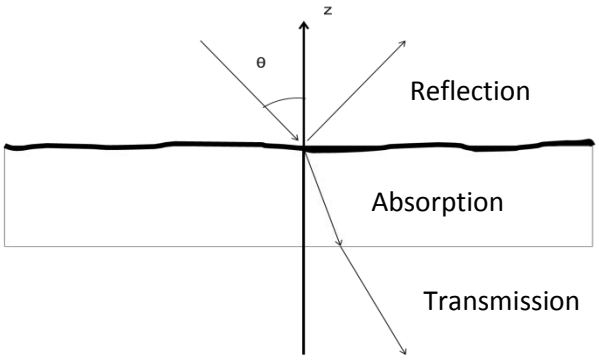

Figure 9. Schematic of the interaction of a laser beam with a metal substrate [29]

The beam will be partially reflected, partially transmitted and partially absorbed. In the case of a metal, the bulk transmission is effectively zero. Here the absorptivity equals the

emissivity and the reflectivity is equal to 1 – emissivity. The absorptivity of materials to laser energy is affected by the wavelength of the laser used and the temperature and roughness of the substrate material. As the temperature of the material rises there will typically be an increase in absorptivity [30].

An Nd:YAG laser is a solid state laser which emits a beam of wavelength 1.06 microns [9]. A fibre optic delivery system transports the laser beam from the source to the focusing lenses so that the desired spot size can be focused on the target location. Although the energy distribution in a cross section of the laser beam will differ from case to case, in practice it can be approximated as a Gaussian distribution which is usually used to simulate the intensity and energy distribution of mono-mode laser radiation [31].

It can be described as;

$$I(r)=I_0 exp((-r^2)/(R^e_s)^2) \qquad \text{Equation 2}$$

where r is the radial distance from the centreline of the beam and R is the radius of the beam.

The laser beam strikes the material and increases the temperature of the interaction area until it melts and then vaporises. The material around the irradiated area is heated up through conduction [30].

Heat is essentially related to the kinetic energy of molecules. The higher the temperature of a material, the greater the thermal agitation of the constituent molecules [32]. Regions which contain greater molecular kinetic energy transfer this energy to regions with less kinetic energy by conduction, convection and radiation, which may occur separately or in combination. Assuming that the material is homogeneous and isotropic, the temperature distribution can be described by the heat conduction equation;

$$\rho c \frac{\partial T}{\partial t} = k\nabla^2 + \varepsilon I(x,y,z,t) \qquad \text{Equation 3}$$

where ρ is the density, c is the specific heat and k is the thermal conductivity of the material. ε is the absorptivity and $I(x,y,z,t)$ is the laser energy delivered per unit time and unit volume of metal. In practice there are many other variables such as temperature-dependant material properties, phase transformations, heat loss via radiation or convection and moving heat sources, but this equation is the basic governing equation [16].

2.3.2.2 Analytical modelling of heat transfer

As laser material processing has been developed, mathematical modelling has been used as a tool to help the understanding and control of the process. Classical heat transfer theory is used to analyse the heating/cooling during laser processing [9].

Mathematical modelling can be a powerful tool in improving the quality and speed of production if it is able to predict the outcome of altering key variables. Heat transfer can be described mathematically if the thermal properties and boundary conditions are correctly defined, allowing for the assumption that material properties are independent of temperature.

Heating during DLD is a non-isothermal process, characterised by high peak temperatures, high temperature gradients and rapid temperature fluctuations. An analytical approach makes it possible to derive relatively simple equations to understand the temperature-time pattern, but the complexity of heat flow phenomena demands validation of predictions against numerical calculations and *in situ* thermocouple measurement [33].

Heat loss by radiation and convection from free surfaces are usually negligible in DLD. The fundamental uniaxial differential equation for heat conduction in solids can be derived from Equation 3 to be;

$$\frac{dT}{dt} = a\frac{d^2T}{dx^2} \qquad \text{Equation 4}$$

where *T* is temperature, *t* is time, *a* is thermal diffusivity and *x* is the heat flow direction.

Simple analytical solutions assume that material thermal properties are constant and independent of temperature, but this is unrealistic as λ, *a* and ρc all vary significantly with temperature and are also dependent on the thermal history of the base material.

Thermal diffusivity (*a*) is related to the thermal conductivity (λ) and volume heat capacity (ρc) by the equation;

$$a = \lambda/\rho c \qquad \text{Equation 5}$$

These limitations can be overcome and the accuracy of the solution improved by using reasonable average values within a specific temperature range.

To model DLD it is assumed that the heat source moves at a constant rate along a straight line and that the net power supply is constant. Observation has shown that zones of temperature below the melting point remain at constant width, and the temperature field around the source will not vary with time, considered as pseudo-steady state. This largely simplifies mathematical modelling of heat flow, though it imposes restrictions on the model. A simple model for a line heating model is shown in Figure 10.

If It is assumed that heat is released instantly at time t=0 at an initial temperature T_0, in a line, the following equation for a line source can be used;

$$T - T_0 = \frac{Q/d}{\rho c(4\pi a t}\exp\left(-r^2/4at\right) \qquad \text{Equation 6}$$

where Q is the net heat input released at t=0.

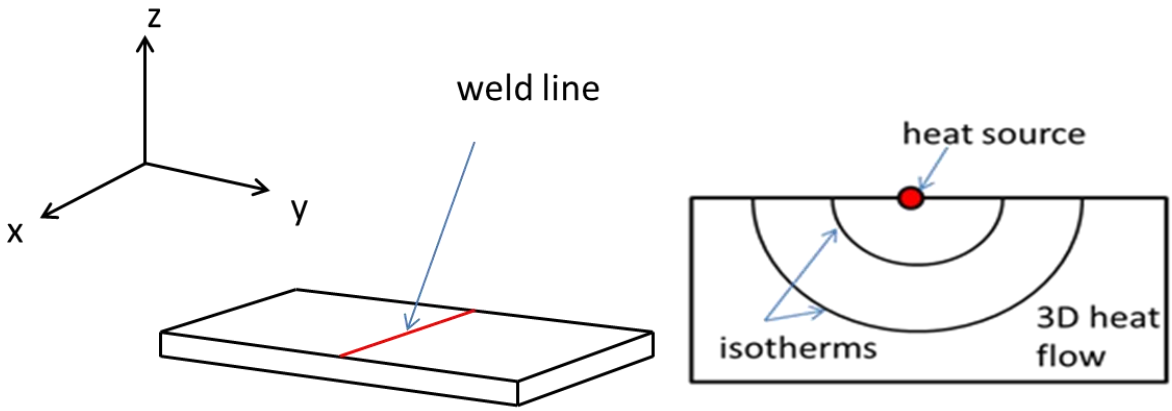

Figure 10: An instantaneous line source model is used for assessment of laser interaction in DLD.

In reality the cooling of the deposited material can be more closely likened to a feedback path which includes the current deposit geometry contact with substrate, thermal history, stress development and adherence to the substrate. These complexities reduce the accuracy of simple models [34].

2.3.3 Microstructural evolution

In DLD the heat affected zone (HAZ) is small. The size of the molten pool has an effect on final microstructure because a smaller melt pool will have a higher cooling rate [35]. A high

cooling rate leads to finer grain size and suppresses the formation of secondary phases, producing a more homogeneous microstructure and in some cases leading to the formation of metastable phases [36]. Refined microstructures usually result in corresponding improvements in mechanical properties.

The shape of the melt pool is influenced by the flow of heat and metal, with melting occurring ahead of the heat source and solidification behind it [33]. The heat input determines the volume of molten metal, as well as thermal conditions under which solidification takes place. The crystal growth rate is related to the cooling rate, which depends on laser travel speed and melt pool shape.

Initial solidification during DLD takes place epitaxially, where the partly melted base metal grains at the fusion boundary act as seed crystals for the columnar grains (see Figure 11). The solidification microstructure depends on the grain coarsening behaviour of the base material, so when laser power is high the grain growth of the base metal can be considerable and the size of the columnar grains at the fusion boundary will be correspondingly coarse. During multiple passes the columnar grains can re-nucleate at the boundaries and subsequently grow across the entire fusion zone [33].

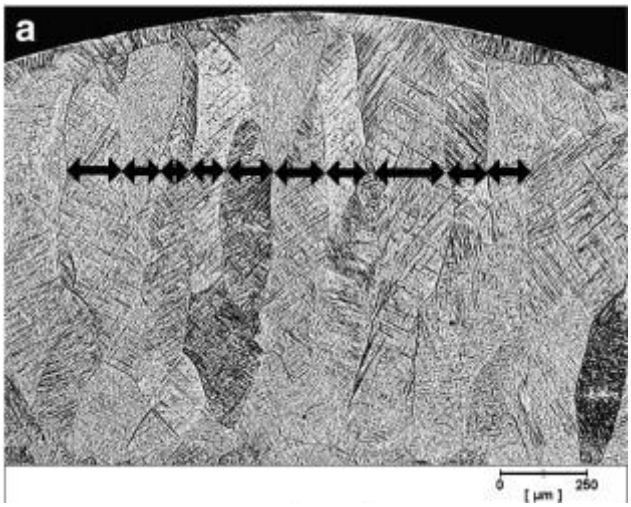

Figure 11: The growth of columnar grains in a Ti-6Al-4V component [37]

Growth of columnar grains is always close to the direction of the maximum thermal gradient in the melt pool i.e. normal to the fusion boundary, implying that columnar grain morphology depends on melt pool geometry pool. Melt pool geometry is a function of laser scanning speed and the balance between heat input and cooling conditions. A tear shaped melt pool is characteristic of fast-moving, high power sources, or of a material with low thermal diffusivity, whereas an elliptical melt pool is characteristic of a low power, low speed source.

2.3.3.1 Phase changes and grain growth in Ti-6Al-4V

A model has been created to evaluate the effect of the thermal profile of the melt pool on the microstructure of a component made from 316 stainless steel using DLD. From this it was found that the highest quench rate occurred when the lowest laser power was used. The cooling rate at the highest power was lower so a coarser grain structure is expected [26]. This means that the cooling rate of the molten pool determines the grain size at the

nuclei but not the final microstructure of the material as it will be affected by the temperature history of the process if a phase transformation occurs.

Characterisation of the forming mechanisms, microstructure and mechanical properties of titanium alloys are a research area of significant interest for the future development of industrial applications for DLD. It has shown that laser-deposited Ti-6Al-4V has a number of differing mechanical properties when compared to otherwise similar wrought product. These are higher strength, lower ductility and more distinct anisotropic properties [38]. A similar study found that laser power, scan speed and powder feed rate have a large effect on the structure of the deposited Ti-6Al-4V. It was also noted that predicting the size of these large grains was difficult due to the variable nature of the substrate to act as a heat sink [39].

A detailed study revealed that tensile strength of direct laser fabricated Ti-6Al-4V components at room temperature could be increased by using heat treatment to control the microstructure [40]. The formation of defects in titanium alloys were also examined using microscopic analysis, which revealed two types of defect – porosity and ill-bonding between layers. Porosity was found to be spherical and randomly distributed as a result of powder manufacturing methods and ill-bonding was irregular in shape and found to be directly influenced by laser energy density, layer overlap and z axis retraction rate.

A microstructure-evolution map was developed to consider peak temperature and cooling rate in order to qualitatively determine the transformations that may form during the DLD processing of Ti-6Al-4V [36]. This map showed that a large region of mixed martensite and α phase should be present, according to the input thermal history. However, experimental observation showed little martensite and the microstructure was instead dominated by Widmanstätten α. This difference may be due to the simplification of the heat source, as a

constant peak temperature has been assumed, which will not be attained using an Nd:YAG laser.

Managing the thermal history is crucial for determining the microstructure and ensuring that the correct material properties are present for the application. Suggestions have been made that forced cooling could be combined with thermal modelling in order to control microstructural growth, but experimentally it has been shown, though not satisfactorily explained, that induced heating of 200°C is more successful for creating a coherent microstructure [41].

2.3.3.2 Process models for heating/cooling rates and microstructure

Numerical modelling methods can be used to study thermal evolution as an effective method for understanding microstructural evolution and residual stress. There have been many thermal models established but they are designed according to specific experimental facilities or with particular assumptions. As yet there is no comprehensive model which can be applied to DLD available in the public domain. There are however a number of useful models that consider separate elements of the process.

The ability to accurately predict how Ti-6Al-4V components will develop under a wide variety of manufacturing conditions is crucial for future large scale development. Early models for predicting thermal history of laser formed Ti-6Al-4V help to predict the microstructure that may form as the result of complex thermal histories that are developed during the layering process [29].

Another microstructural model was developed to look at Ti-6Al-4V deposited using a TIG weld build-up process [42]. This was able to consider a number of variables including the

phase volume fraction of α, β, Widmanstätten α, grain boundary α, martensite α and the α lath thickness. It was also able to consider the cyclical heating effect but was unable to account for grain growth. A further model attempts to predict both the shape and thermal loading of parts manufactured by direct laser deposition using a numerical-analytical approach [43]. It involves an FEA software package and is able to describe the moving melt pool. As a result it is possible to provide an accurate prediction of the temperatures near the melt pool, the thermal cycles and melt pool dimensions when constructing a 25 layer high wall from titanium alloy.

A great deal of useful work has been done in attempting to model the complex processes that occur during DLD of metals in order to better understand the resulting microstructure an therefore mechanical properties of the deposited materials. The next steps will include expanding a model to encompass a complex DLD component made up of hundreds or even thousands of layers. However, this is a great challenge as a research topic as the behaviour of the base plate and newly formed component as a heat sink is currently not well understood [22]. For large components fabricated by DLD, the heat sink effect would be very pronounced.

2.4 Distortion and residual stress

Direct laser deposition causes distortion due to the localised heating which leads to thermal expansion, in a very similar way to welding. When the laser heats the substrate, the heated metal expands into the unheated metal. This stress is larger than the yield stress of the material and the unheated substrate is deformed plastically [44]. When the heat source moves along the substrate the heated material begins to cool and contract. As the plastic

deformation is permanent, the substrate is forced to bend by the residual stresses introduced upon cooling, as shown in Figure 12.

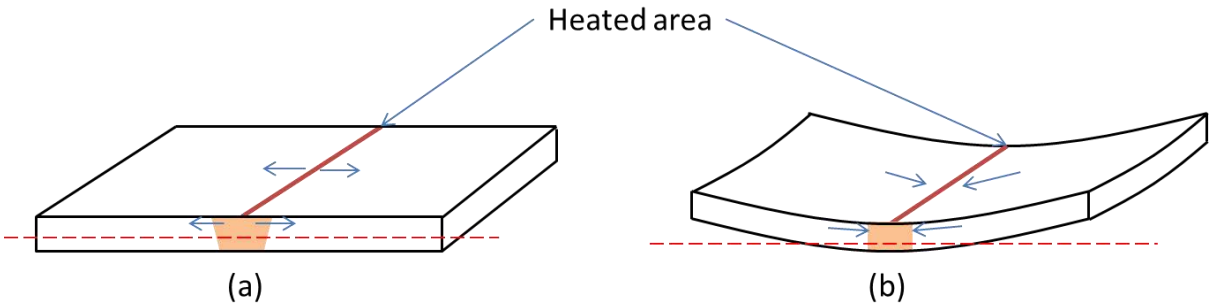

Figure 12: (a) Tensile stress caused by thermal expansion of metal and (b) resulting compressive stress from the plastically deformed region

2.4.1 Introduction of residual stresses during DLD

Residual stresses are introduced into a material after the uneven heating and cooling that takes place during laser processing. This can lead to surface or subsurface cracking of the processed components [44,45,46] and distortion of the finished component [46]. Heat treatment is required to relieve residual stresses, which might reduce the attraction of DLD as it adds an extra processing step. For this reason the ability to predict and control residual thermal stress fields is highly desirable.

The large concentrated heat flux rates that allow a laser to melt materials efficiently also result in large localised thermal stresses in a small heat affected zone. These thermal stresses can lead to micro-cracks, a decrease in mechanical strength and fatigue life and the possibility of catastrophic failure of the component while in service. Studies have been undertaken to assess the stresses which occur during laser processes, investigating selective laser sintering [48,49] and shaped metal deposition [50]. Through finite element modelling

and experimentation these studies determined that final distortion could be reduced by substrate pre-heating, which reduces the thermal gradient, and by rigid bolting of the substrate. Clamping the substrate firmly against the work surface means improves the ability of the conduction of the heat across this boundary, creating a lower thermal gradient than if the substrate were insulated by the surrounding atmosphere.

Another model examined thermal interactions of droplets deposited on top of one another. Thermo-mechanical models of temperatures and stresses were considered, and convection and radiation conditions imposed on the top surface and a constant temperature condition imposed on the bottom surface were given as boundary conditions. The simulation used temperature-dependant thermal properties of stainless steel and considered latent heat released during solidification. The results from deposition in a discrete path demonstrated the importance of process-induced preheating in reducing residual stress. Therefore, process-induced pre-heating could be increased by using insulated base plates and by choosing optimal deposition paths [51].

Although some work has been done on residual stress introduction during DLD and similar processes, residual stress due to transformation plasticity is usually neglected due to both the complexity involved and the inability to measure the contribution of each phase constituent in this entire transient phenomenon. However, simulations carried out for certain locations have shown that residual stresses due to phase transformation plasticity are significant, especially at the substrate-deposit interface [51,52]. These could then lead to crack formation and eventually to the de-bonding of the deposited material under conditions that would otherwise be predicted to be safe if phase transformation effects are discounted.

As the DLD process has many similarities with welding, it is useful to look at data presented on welding for suggestions on the shape and magnitude of residual stresses. Figure 13 shows the stress distribution both across and along a weld line.

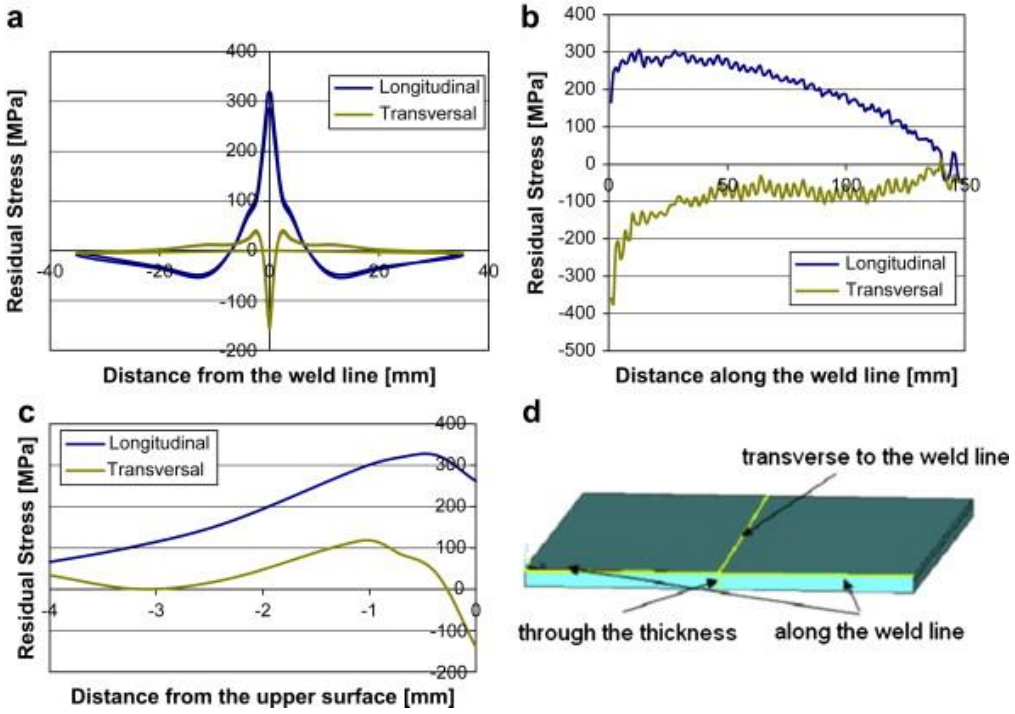

Figure 13: Residual stress distribution for steel plates a) transverse to weldline, b) along the weld line and c) through the plate thickness [53].

2.4.2 Controlling distortion

The most common method of predicting stresses introduced by DLD is by finite element modelling, due to the limitations of experimental stress measurement during laser processing [55,56,57]. Several studies have been carried out specifically to look at the residual stresses and distortion caused by DLD.

The deposition process involves temperature gradients and so thermal stresses develop. Therefore the key to advancing the DLD process is improving understanding of how residual stresses develop. Process changes such as substrate pre-heating and various deposition paths have been proposed and compared to look at the effect on distortion and residual stress. A combination of substrate preheating to reduce initial thermal gradients and substrate insulation to exploit the preheating by the process itself has been shown to significantly limit residual stress-induced distortion [58].The deposition pattern can also have a significant effect on the part stresses and deflections [59].

Pre-heating has been studied further as it can be used to reduce residual stresses and also create a more consistent microstructure. The effect of base preheating, temperature dependent material properties and the influence of the time between layers have been investigated and it was found that the best results are obtained when a short time delay between layers was allowed to prevent steep changes in the temperature gradient [60]. Also, residual stresses from narrow laser beam processing with high stress gradients can be decreased without additional equipment by defocusing the beam and applying it after processing to regions a certain distance either side of the build line [61].

2.5 Summary

Thermal control has proven to be critical in DLD, both for obtaining consistent microstructures and limiting the effect of residual stresses on component geometry and strength [61]. This justifies the objective of this project that is to better understand the influence of temperature on the DLD process and to study the relationship between cooling rate and distortion.

3 Experimental methods

The aim of the experimental work is to assess the effect of varying thermal conditions during direct laser deposition on the microstructure and distortion of Ti-6Al-4V components. Specifically it is intended to produce thermal data by measuring temperature changes during laser processing over a range of conditions and to measure the distortion which occurs.

3.1 Design of experimental work

The experimental work measures the cooling rates and distortion so that a relationship between the two can be accurately described. The initial work done is included to show the techniques used to test some assertions from the literature review.

Trial Group	Reasoning	Section
Parameter optimisation for primary structures	Familiarisation with equipment and process	appendix
Thin walls	Walls built to allow specimens to be cut for mechanical testing (to be compared with others made using similar manufacturing processes)	chapter 3.1.1
Parameter optimisation for repair	Investigating the definition of optimal repair qualities and changes needed in parameters to	appendix
Thermal management	Controlling the temperature during processing to assess the effect on microstructure	chapter 3.1.2

Table 4. Summary of experimental work carried out using direct laser deposition

3.1.1 Initial work done using DLD

At the beginning of this project there was also an interest in primary structure building using DLD. Work was carried out in support of a Technology Strategy Board (TSB) project, and the work undertaken as part of this research project is detailed below.

Primary structures were built at BAE Systems which acted as a way of becoming familiar with the laser deposition equipment and the general behaviour of deposited Ti-6Al-4V. Parameter optimisation trials were carried out (see Appendix) with the aim of producing thin walls of DLD Ti-6Al-4V with a fully dense microstructure. The thin walls were cut into sub-size mechanical testing specimens as described in ASTM E8 [62].

Identically sized specimens were provided by Exeter University in order to examine the difference in mechanical properties that could be attributed to the manufacturing method. This batch of specimens was made using a four axis laser and, unlike the specimens made at the ATC, the direction of the laser beam was not constant. The mechanical testing was done as part of this research project because the resulting information on potential tensile strength could be used to justify the use of DLD for Ti-6AL-4V builds and repairs. The current literature suggests that tensile strength as high as that of rolled plate can be achieved using DLD.

The failure mechanisms of the samples are also relevant as the literature asserts that DLD components can be subject to directionally dependent mechanical properties [24]. This was examined by cutting the tensile test specimens in different orientations from the DLD thin wall parts.

3.1.2 Investigating cooling rates and distortion

The 4mm thick Ti-6Al-4V rolled plates used to investigate cooling rate and distortion are intended to represent small aerospace components which have suffered damage or wear either in service or during manufacture. To simulate this, each plate has a groove machined in its centre with dimensions 75x10x1mm depth (see Figure 14).

In order to produce valid results the experimental conditions need to be highly controlled and fully instrumented. The thermal boundary conditions have been chosen to cover a wide range of temperature values with the expectation that this will produce results which indicate which conditions are optimal (see Table 3).

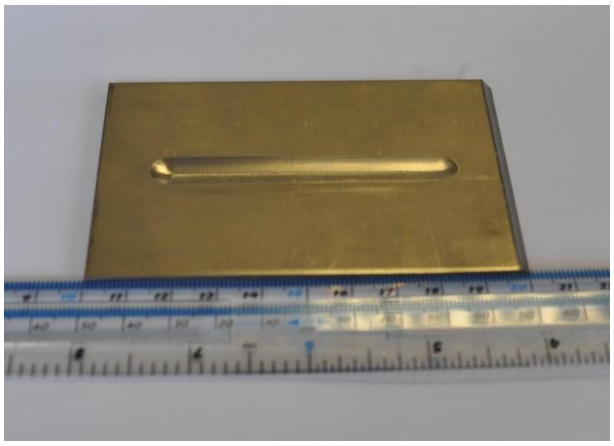

Figure 13 – A machined plate before DLD

Name	Conditions
Plate 1	Heated (200°C)
Plate 2	Unclamped
Plate 3	Insulated
Plate 4	Cooled (10°C)
Plate 5	Clamped

Table 3 – Experimental conditions

When controlling the temperature of the substrate it is clamped down to ensure good contact with the heating/cooling elements. To consider the potential effect of heat being lost through contact with the work surface, one experiment was carried out with a sheet of insulating material clamped between the plate and the work surface. In order to examine

the effect of the clamping, the experiment was also carried out without forced temperature control with the plate clamped directly to the work surface and again with the plate unclamped.

3.1.3 Materials preparation

Each plate was prepared by drilling 0.51 mm holes, 2 mm deep, in which to locate twenty-two 0.5mm K-type thermocouples. The thermocouples were placed in two circles around the groove at distances of 2mm and 5mm from the processing area, and at each corner of the plates (see Figure 15).

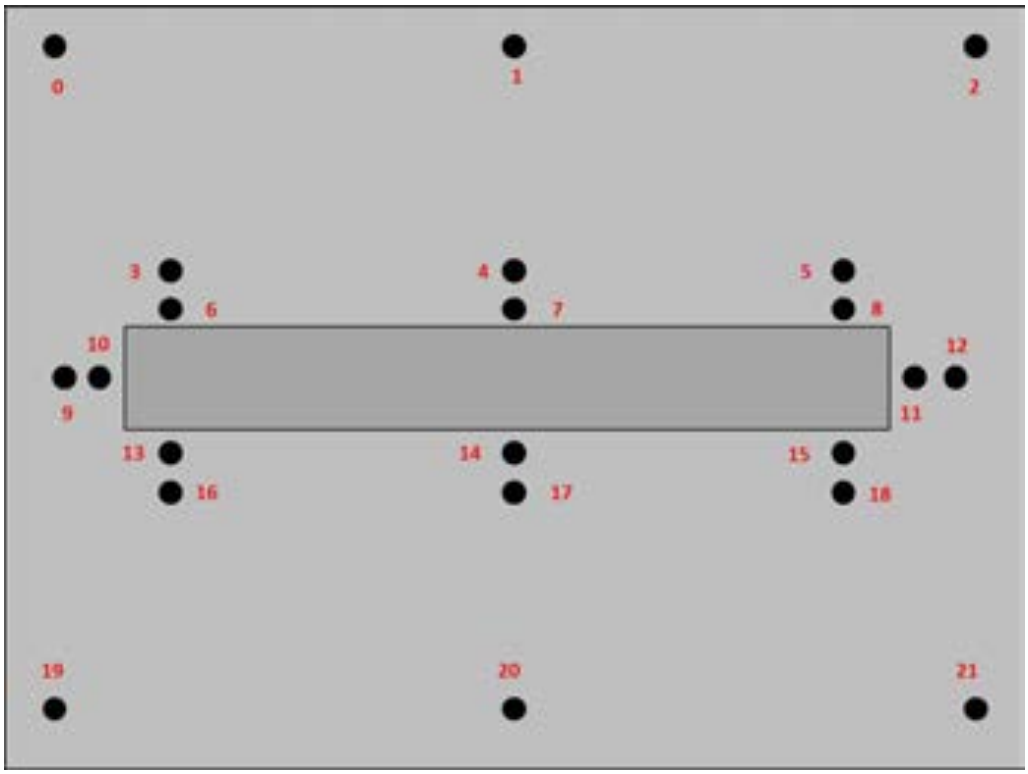

Figure 15 – Position of holes drilled to locate thermocouples

Ideally the thermocouples need to be as close to the heat source as possible in order to get the most accurate data, but it was unknown if they would be able to survive at the temperatures produced by the laser. Also, by having an outer ring of data it is possible to look at the heat transfer across the plate over time. The locations at the very edge of the plate can be used for calibrating the initial temperature with the thermal imaging camera and look at heat transfer over a larger area.

3.2 DLD processing with instrumentation

As the focus of this project has shifted towards repair applications of DLD, work has been undertaken to look at the repair capability at the ATC and methods to improve repair quality. Instrumentation of the process allows validation of assumptions and quantitative comparison.

3.2.1 Processing equipment

Each plate was positioned inside the environmental control bag using locating screws (see Figure 16). The thermocouples were arranged into the correct locations and labelled so that the readings could be identified.

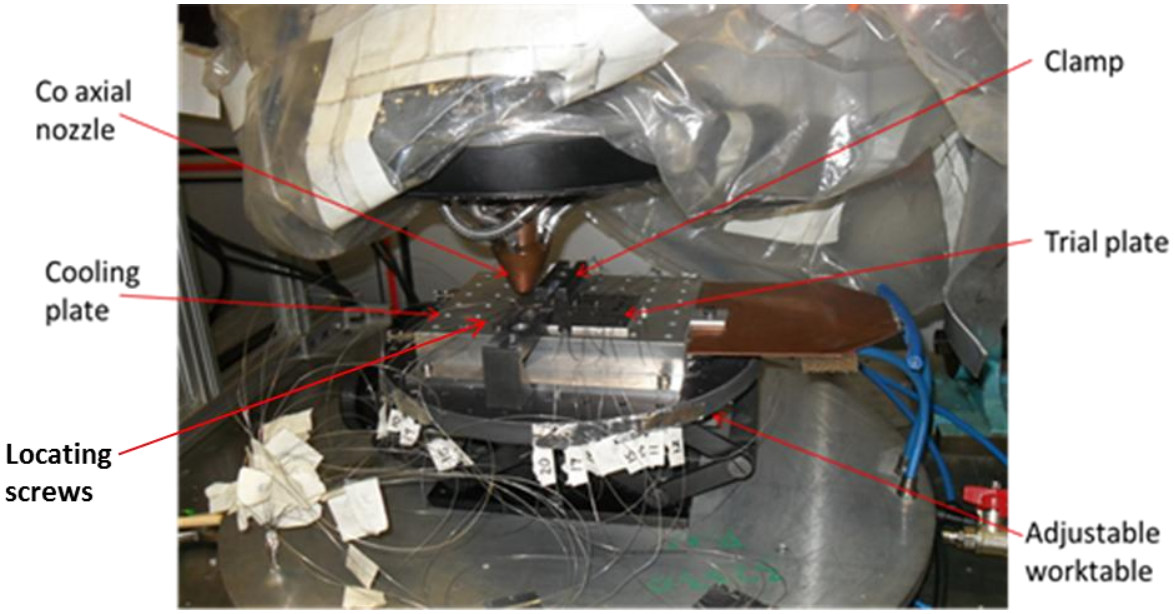

Figure 16 – Set up for processing a plate inside the environmental control bag

The bag was secured around the bottom of the table using a rubber o-ring to seal it. This created an environment which could be filled with protective argon, with a small tap to allow oxygen to escape out of the top.

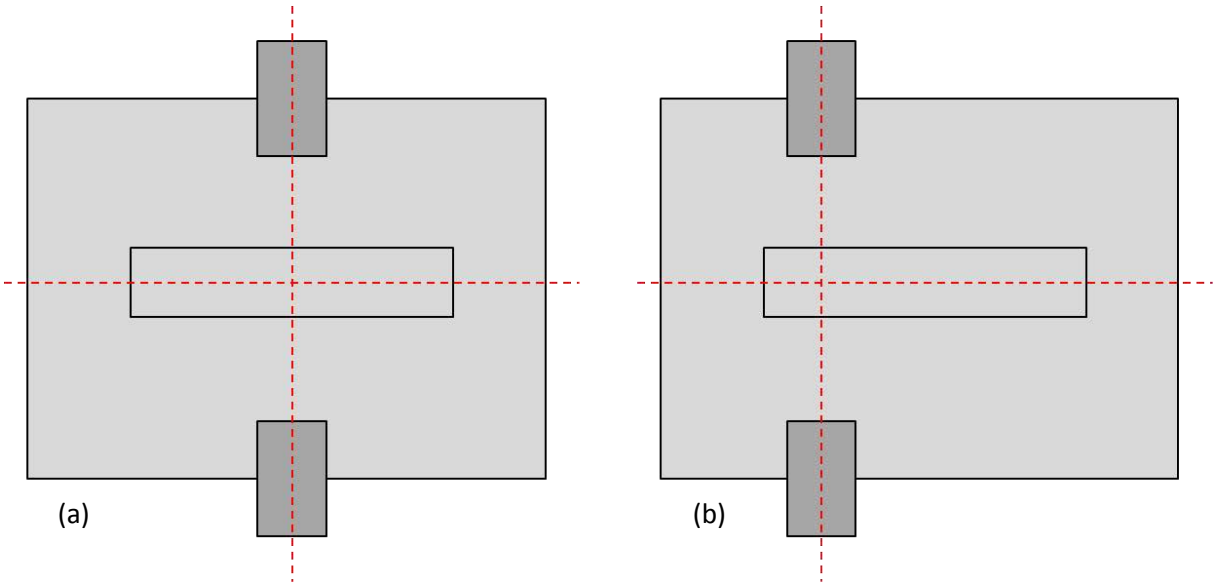

Figure 17 – The (a) proposed and (b) actual position of the clamps used during DLD proposing

Figure 17 shows that the actual clamping arrangement used was symmetrical about the x axis but not the y axis. The intention was that the arrangement shown in (a) should be used but the position of the thermocouples (see Figure 15, locations 1 and 20) meant that this was not possible. The change to the proposed clamping arrangement is expected to have an effect on the distortion of the plates and this is discussed in the next chapter.

When the environmental control bag is sealed, there is a transparent window in the front through which the digital camera can record the processing. The rest of the bag is transparent to the thermal imaging camera, so that is positioned to the side of the cell to record the processing at a slightly different angle. The nozzle inside the bag is controlled by the overhead gantry and is able to move on three axes.

3.2.2 Measuring heating and cooling rates

Temperature measurements were taken using thermocouples and a thermal imaging camera to determine the thermal history of the deposited material and substrate. The thermocouple measurements were taken at a frequency of 60 Hz and the thermal imaging camera operated at 30 Hz. These measurements have their limitations as a thermocouple is used to measure a molten pool temperature but is very difficult to locate in the centre of the molten pool. Also, thermal imaging cameras require known values of emissivity to calibrate them, so while it is possible to measure the molten pool temperature it is difficult to obtain temperature profiles away from the molten pool due to unknown and varying emissivity of the rough surface of a DLD component.

A set of equations for calculating cooling times after DLD have been proposed, based on those used for arc welding [33]. These have been used on sample data in order to test the validity of the equations and assumptions that have been made.

The data used below is for plate 3, thermocouple location 7 and the aim is to calculate the cooling time from 500°C to 200°C. This time is known to be 95 seconds from thermocouple readings during experimentation.

It is convenient to write the equation in dimensionless form;

Dimensionless temperature

$$\theta = \frac{T - T_0}{T_c - T_0} \qquad \text{Equation 7}$$

where T_c is the chosen reference temperature. In this case the melting temperature of 1650°C is used and the ambient temperature T_0 is taken to be 20°C.

$$\theta_{500} = \frac{500 - 20}{1650 - 20} = 0.295 \qquad \text{Equation 8}$$

$$\theta_{200} = \frac{200 - 20}{1650 - 20} = 0.110 \qquad \text{Equation 9}$$

Dimensionless time;

$$\tau_1 = \frac{t}{t_i} \qquad \text{Equation 10}$$

where t_i is the beam ignition time, arbitrarily given as 0.1s for this example.

Dimensionless operating parameter;

$$n_1 = \frac{2Q \times \eta}{\rho c (T_C - T_0)(4\pi a t_i)^{\frac{3}{2}}} \qquad \text{Equation 11}$$

where Q = beam power, η = beam efficiency factor, ρc = volume heat capacity and a = thermal diffusivity.

(The beam efficiency factor is estimated to be 0.3 for the purpose of this calculation, and thermal properties are assumed to be independent of temperature.)

$$n_1 = \frac{2(400000)\times 0.3}{2502950(1650-20)(4\pi\times 2.637\times 10^{-6}\times 0.1)^{\frac{3}{2}}} = 8618.763 \qquad \text{Equation 12}$$

Rearranging the equation for dimensionless calculation gives;

$$\Delta\tau_1 = \left[\left(\frac{n_1}{\theta_{200}}\right)^{\frac{2}{3}} - \left(\frac{n_1}{\theta_{500}}\right)^{\frac{2}{3}}\right] = \left[\left(\frac{8618.763}{0.110}\right)^{\frac{2}{3}} - \left(\frac{8618.763}{0.295}\right)^{\frac{2}{3}}\right] = 959.413 \qquad \text{Equation 13}$$

Therefore time to cool from 500°C to 200°C is given by;

$$\Delta t_{5/2} = t_i \Delta\tau_1 = 0.1 \times 14.570\ s = \mathbf{95.941}\ \text{seconds} \qquad \text{Equation 14}$$

3.3 Microstructure and distortion characterisation

The microstructure of the repaired component is important because it indicates the final material properties. The microstructure of the repaired component should be close to that of the substrate so that the repair is not a weak point in the component. The important microstructural features are the width of the α lamellae and the texture type and symmetry.

3.3.1 Preparing samples for characterisation

After processing, six specimens with dimensions 10mm x 15mm were cut from each plate (as shown in Figure 19) and mounted in epoxy resin. These specimens were polished using increasingly fine grades of Si-C paper and OPS polish, then finally a 1 micron diamond paste to produce a mirror finish.

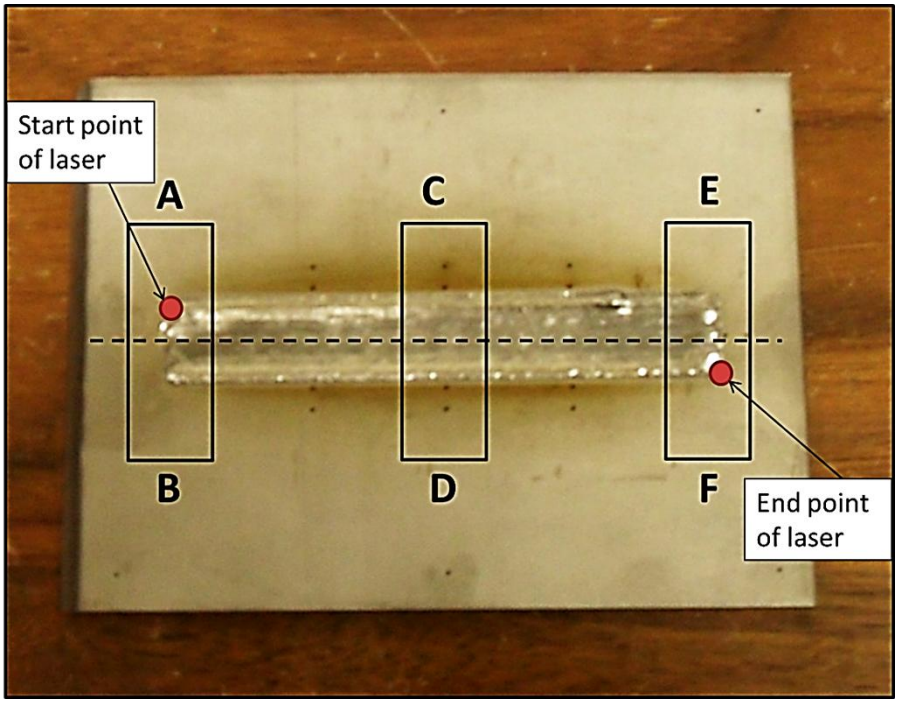

Figure 19: Location of specimens cut from the sample plates.

The final stage in specimen preparation was to etch each one with Kroll's reagent [4]. Each sample was swabbed for around 20 seconds until the surface ceased to be reflective and then washed in distilled water to reveal the grain boundaries and the α particles in the microstructure.

3.3.2 Distortion measurements

It cannot be assumed that the plates used for the experiments are completely flat or identical to one another as some distortion will have occurred when they were cut to size and had the grooves machined into them.

Once the plates had been prepared for DLD processing they were each labelled and a three dimensional laser scan was made. The laser scan collected information about the distance of the plate surfaces from the point of recording and this data was then used to reconstruct a digital image of the plates. After processing the plates were scanned again and the images created were overlaid so that the changes in geometry due to processing could be measured. In this way the distortion of each of the plates could be determined.

The distortion of each plate was expected to be related to the rate at which the plate cools after processing. By plotting the distortion against the distance from the centreline and comparing this to the graphs showing the cooling rate against the distance from the centreline, the relationship between distortion and cooling rate could be inferred.

4 Results and discussion

The initial parameter optimisation trials showed that all substrates undergoing DLD will suffer some degree of distortion and that distortion differs depending on a number of variables. In order to design experiments that are meaningful, these variables needed to be as tightly controlled as is practical. For this reason each substrate used had the same geometry and all were cut from a single rolled plate. The clamping arrangement was marked out beforehand so clamps were always in the same place and the laser scanning path is pre-programmed.

4.1 Process parameter optimisation

The parameters used for building primary structures were initially investigated for repair work as a base from which to begin parameter optimisation. The parameters which were varied included; laser power, focal distance, laser scanning speed, powder feed rate and the amount of overlap of subsequent layers.

The first repair work carried out using these parameters produced quite poor quality results with very high porosity and surface roughness. Systematic trials to vary the parameters and find optimised values were carried out (see Appendix).

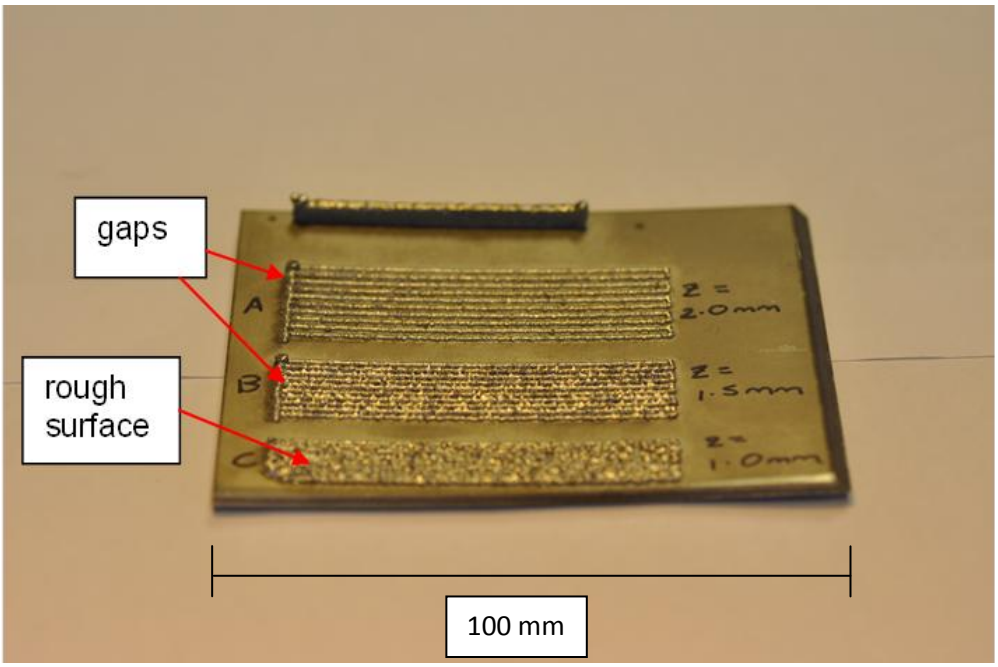

Figure 20: Plate 020910-1: Reducing the distance between overlapping layers of deposited molten Ti-6Al-4V powder from 2 mm to 1 mm

Figure 20 shows a trial plate made for studying the effect of reducing the distance between horizontal layers to produce a non-porous repair. The starting parameters were taken from those found by optimising for building primary structures (see Appendix).

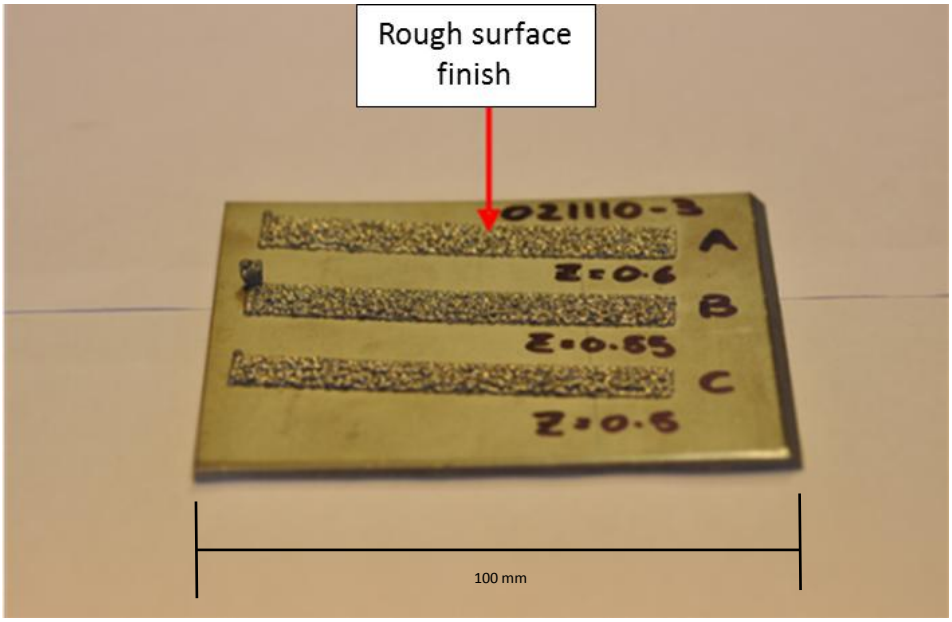

Figure 21: Plate 021110-3: effect of reducing the overlap of deposited layers

As the distance between the layers was decreased the roughness improved only slightly as the finish was very poor (see Figures 21 and 22). Even when the distance was decreased until the layers overlapped, the resulting repair still had a very rough surface and appeared very porous.

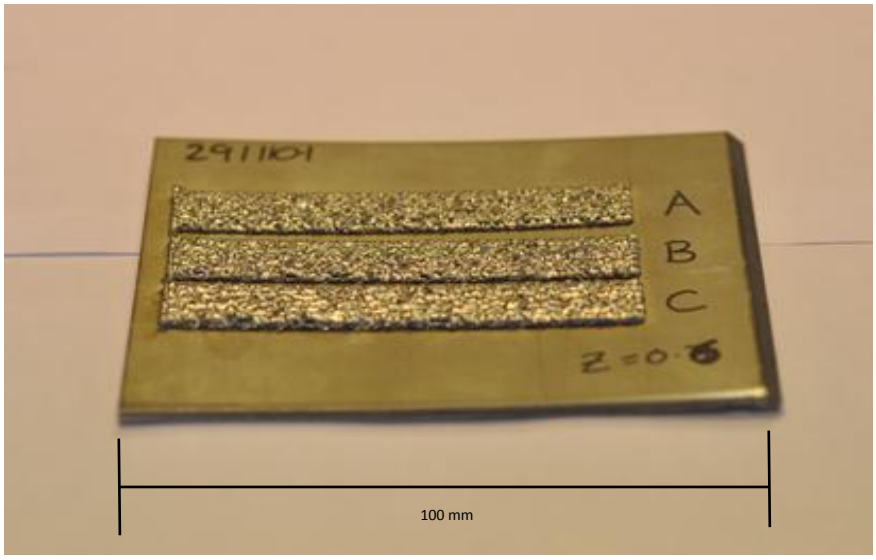

Figure 22: Plate 291110-1: Increasing the laser power through A) 200W, B) 250W and C) 350W at a constant overlap distance of 0.6mm

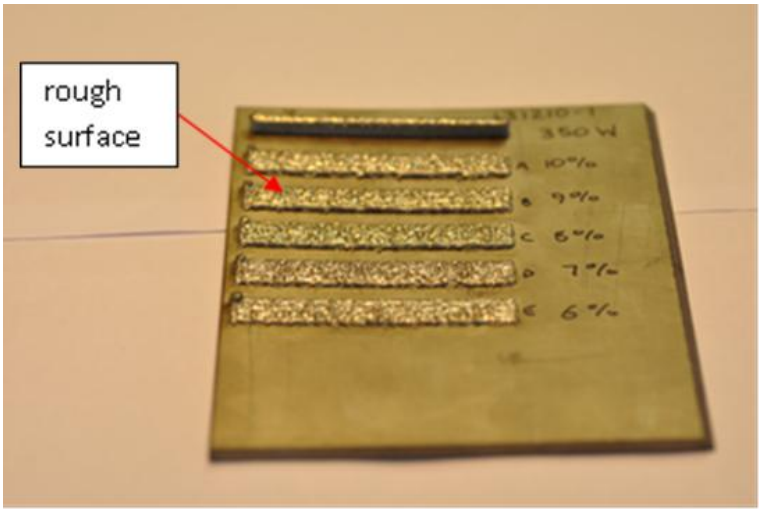

Figure 23 – Plate 131210-1: Decreasing the powder feed rate from 10% to 6% at a constant laser power of 350W

Neither increasing laser power nor decreasing powder feed rate (Figure 23) improved the surface finish of the repairs. Previous work with Ti-6Al-4V has shown that overheating during DLD can cause “balling” which gives a poor repair quality and surface finish. Balling occurs when too much energy is transferred into the deposited material and it is re-melted.

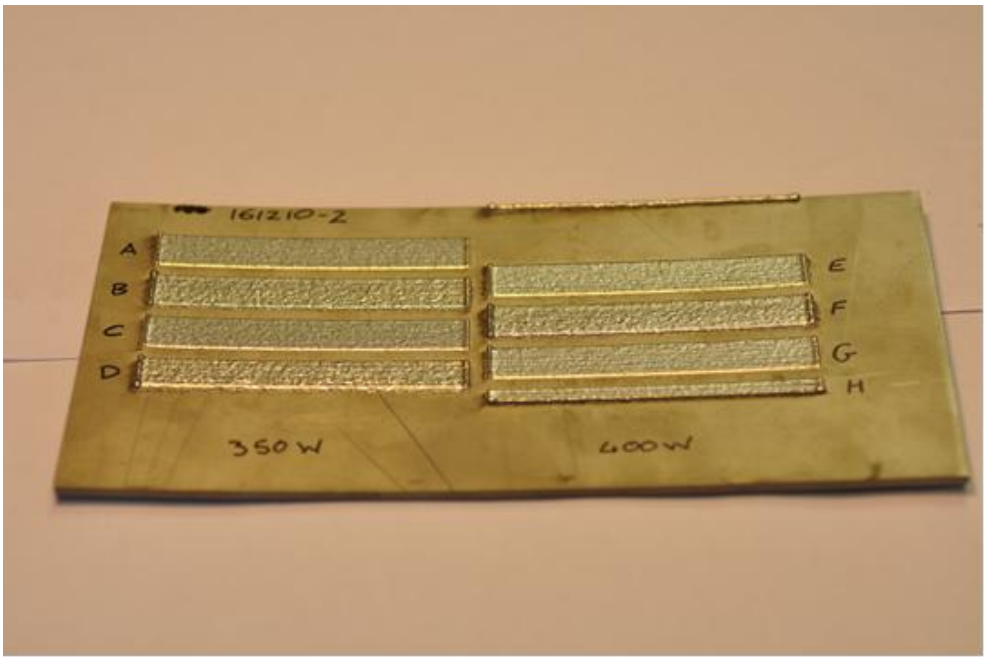

Figure 24 –Plate 161210-2: Increasing scanning speed from 5mm/s to 10mm/s

Figure 24 shows a plate where the scanning speed has been increased from 5mm/s to 10mm/s, reducing both the time in which heat can build up in the substrate and also the overall power being put into the plate. Once an appropriate speed and powder feed rate had been found, the horizontal distance (z) was decreased further to decrease porosity. The optimum parameters for general repair were decided by balancing surface finish, low porosity, good adhesion to the substrate and consistency, shown in Figure 25.

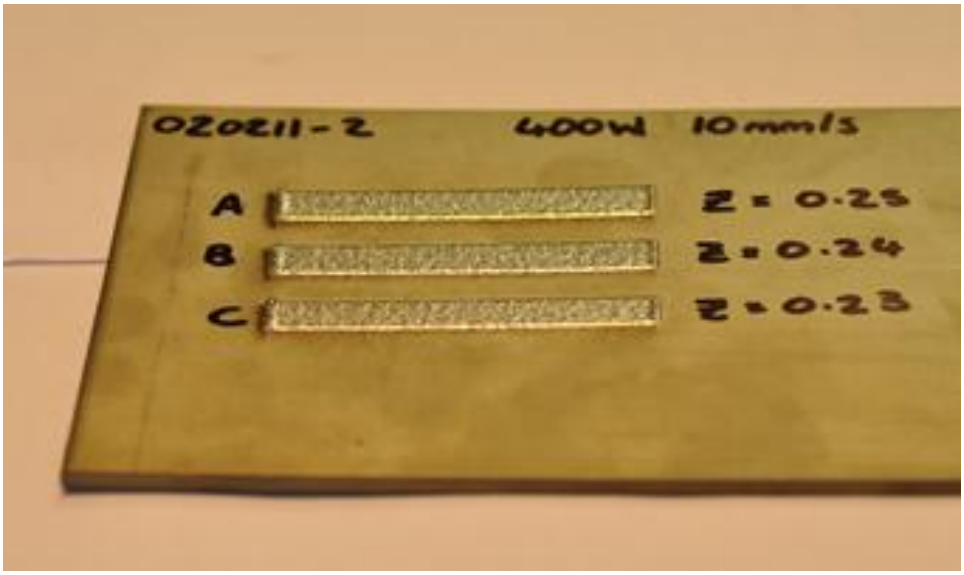

Figure 25 – Plate 020211-2: Reducing the (z) distance to achieve a more consistent finish

4.2 General Observations

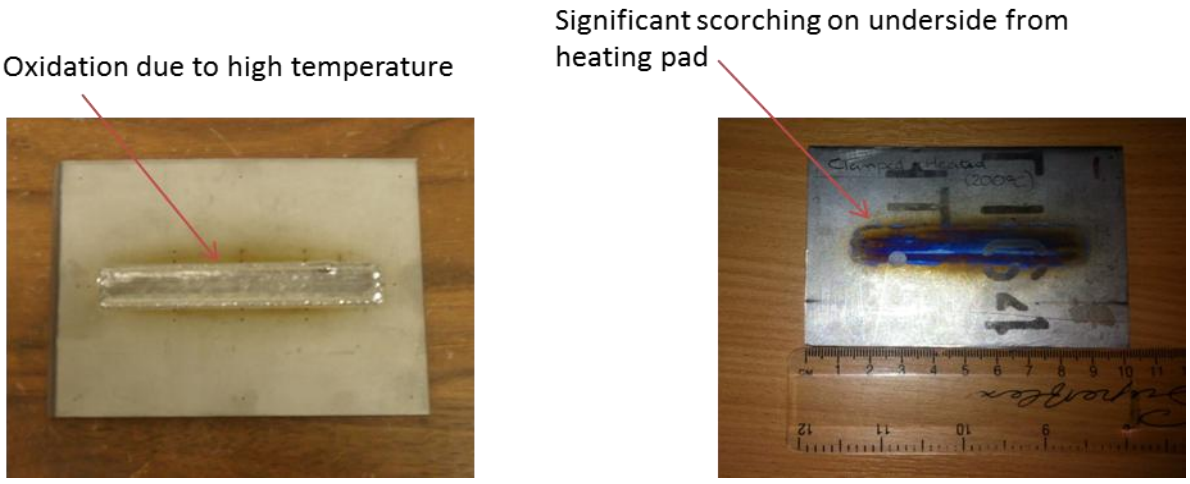

Figure 26: Plate 1 – DLD processed while heated at 200°C

Thermal gradient can be controlled by applying either heating or cooling to the entire substrate. This either heats the entire plate to reduce the gradient between melted and unmelted substrate, or cools the entire plate to minimise the effect of the laser beam. In Figure 26 there is some oxidation visible around the weld area. The oxygen level during processing was monitored and kept below 25 parts per million during processing, but due to the high temperatures achieved the substrate was still hot enough to react with oxygen after 200 seconds, the amount of time each plate was left to cool before turning off the argon shielding.

In Figure 27 the cooling plate has reduced the amount of scorching on the underside of the plate visibly, showing that the heat from processing has not been able to build up in the substrate as much as with the heated plate shown in Figure 26 and the insulated plate shown in Figure 28.

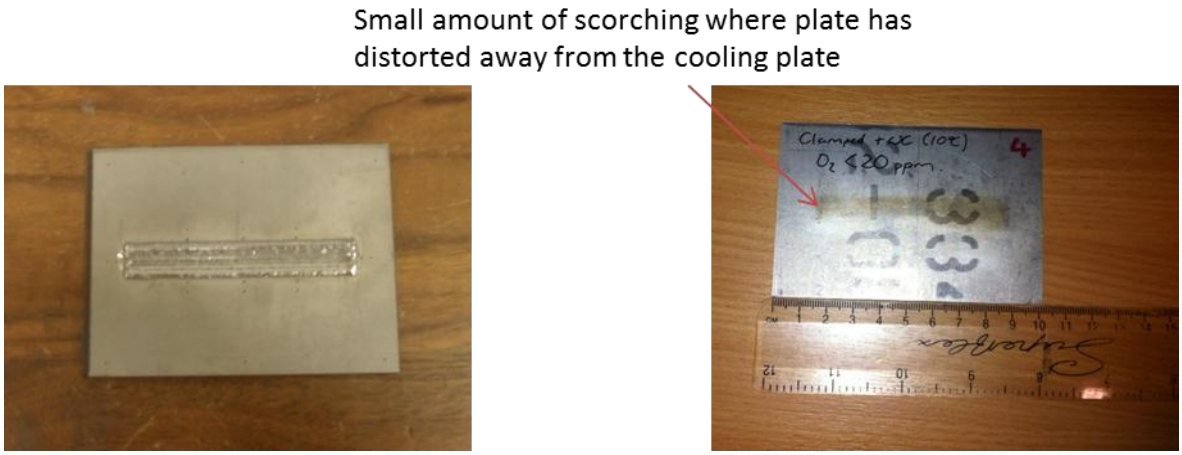

Figure 27: Plate 4 – DLD processed while cooled to 10°C

Where insulation is placed under the substrate the heat introduced by the laser beam will only be able to heat the substrate and not the work surface below, and so the overall temperature of the substrate can be expected to be higher and the thermal gradient therefore lower.

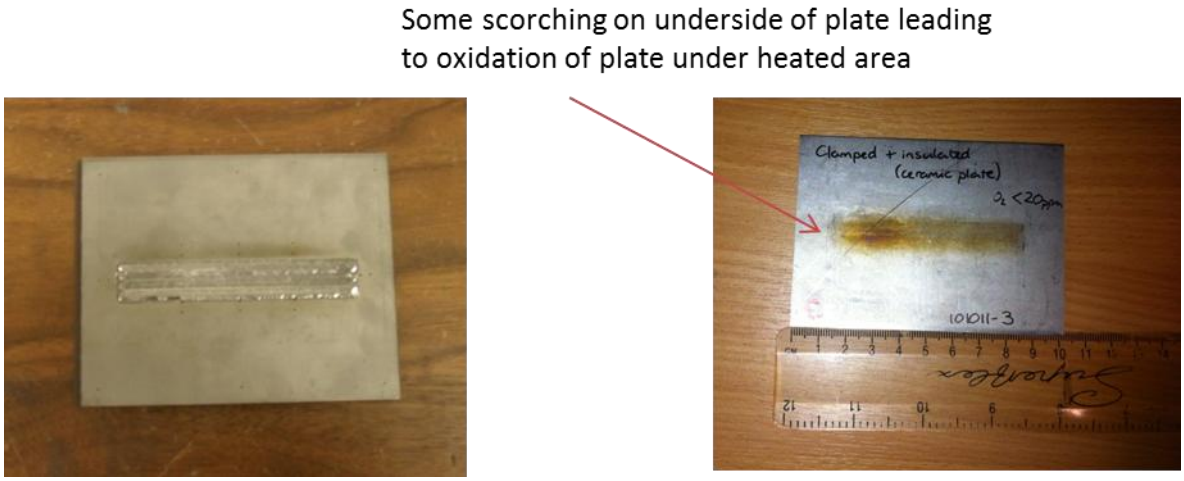

Figure 28: Plate 3 – DLD processed while insulated from the work surface by a ceramic tile

Clamping is important because of the effect of maintaining good and consistent contact between the substrate and surface below. A clamped substrate with no insulation, heating

or cooling applied is included as a control to look at the thermal history at room temperature (see Figure 29).

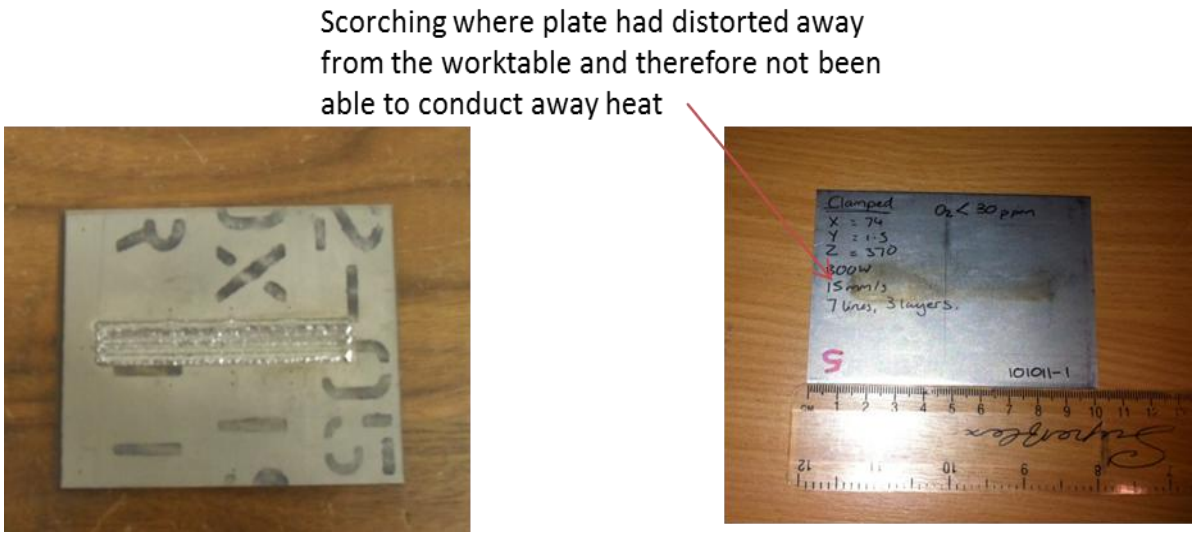

Figure 29: Plate 5 – DLD processed with no temperature control

The unclamped substrate shown in Figure 30 will not have such good contact with the work surface at the beginning of the experiment (no plate can have perfect contact as no surface can be perfectly flat) and the amount of contact will decrease as the substrate distorts away from the work surface upon heating. The argon atmosphere between the substrate and work surface acts as an insulator, so the areas of the plate which have lost contact with the work surface will retain more heat than those which are still in contact.

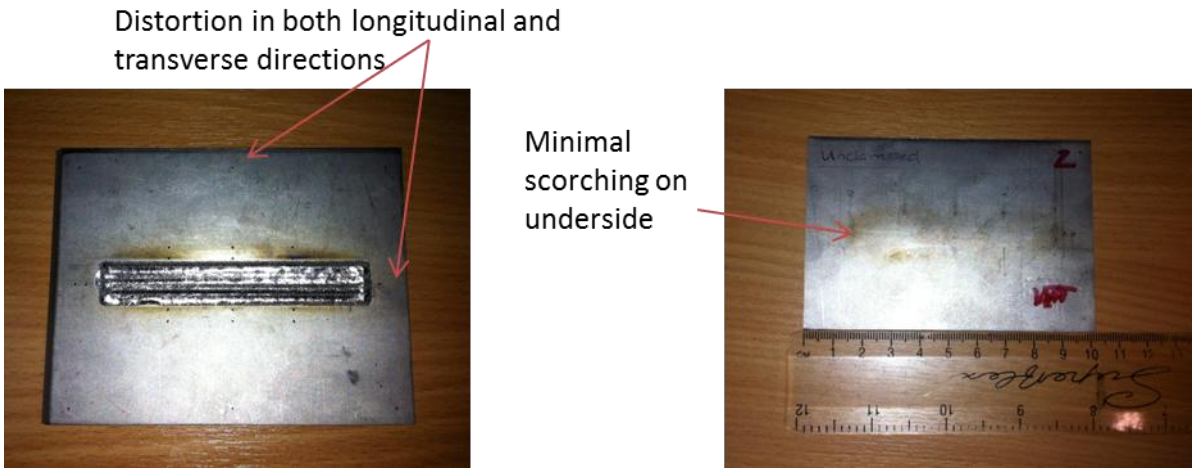

Figure 30: Plate 2 – DLD processed without temperature control or clamping

4.3 Microstructural characterisation

The microstructure developed under the different thermal conditions will control the final properties of the repair. The depth of the heat affected zone and the porosity have been measured at marked locations in each plate so that the effect of changing thermal conditions can be graded.

4.3.1 Defining an optimum microstructure

To some extent, the optimum microstructure of Ti-6Al-4V is dependent on the function which is required from the final component. For the purposes of this project it is assumed the ideal microstructure for a component produced using DLD is one that is at least as strong as the parent material i.e. rolled Ti-6Al-4V plate. This is because the DLD material must not make the repair a weak point in the component.

Rolled titanium plate has small equiaxed grains which gives it good tensile strength In all directions. Figure 31 shows a DLD repair on a rolled plate substrate and the interface

between parent and grown material is clear. Figure 31 (a) shows the grown material at 200x magnification and (b) shows the parent material. The grain size of the grown material is smaller than that of that of the parent material and there is no directional growth except towards the edges of the specimen. There is some porosity in the grown material but there is good consolidation at the interface between parent and grown material. The parent material shows bimodal α+β, showing α grains and transformed α+β.

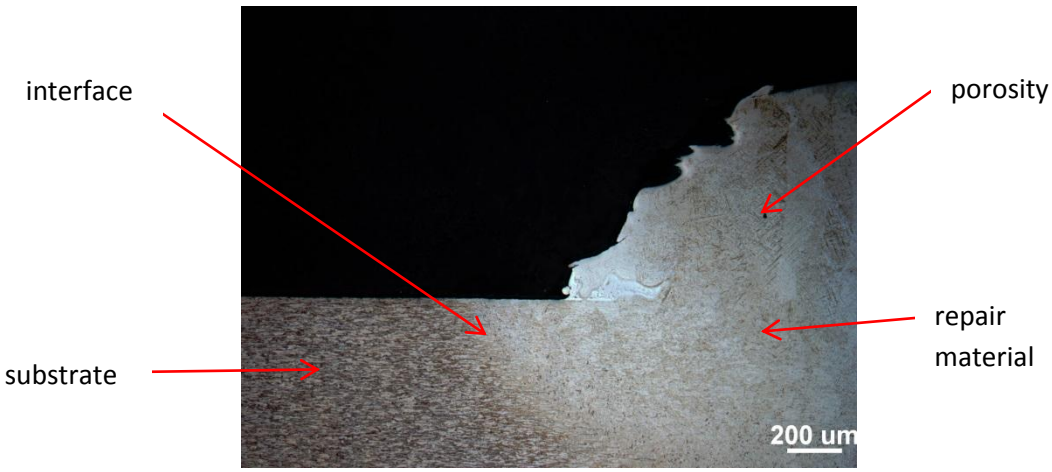

Figure 31: Micrograph showing transition from parent to repair material in the clamped plate (plate 5).

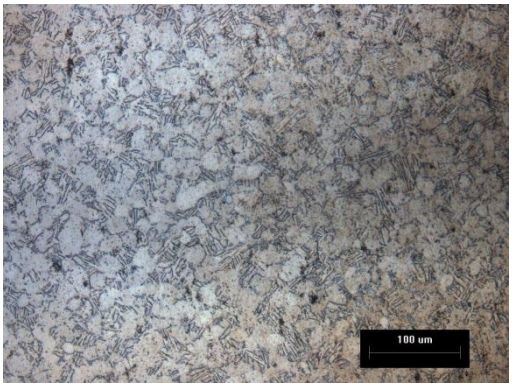

(a)

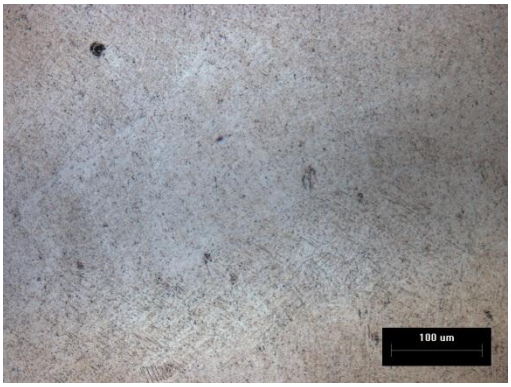

(b)

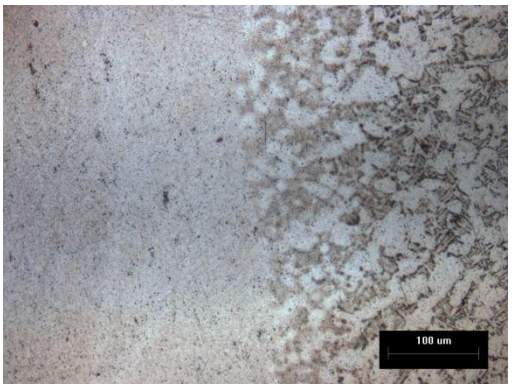

(c)

Figure 32: Micrographs comparing the changes in grain size and structure across (a) parent material (b) deposited repair material and (c) the interface

4.3.2 Examining failure mechanisms

The failure mechanism of tensile specimens made as part of the TSB funded project that was carried out at the start of this research has been examined to find the mechanical properties which can be achieved (see Figures 32-35). This is of interest because it is know from the literature review that the growth of columnar grains resulting from DLD can lead to the introduction of directionally dependent properties [24]

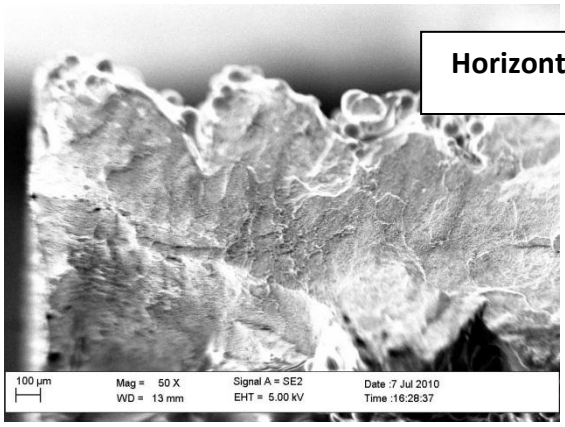

Figure 33: Fracture surface of the horizontal specimen after tensile testing

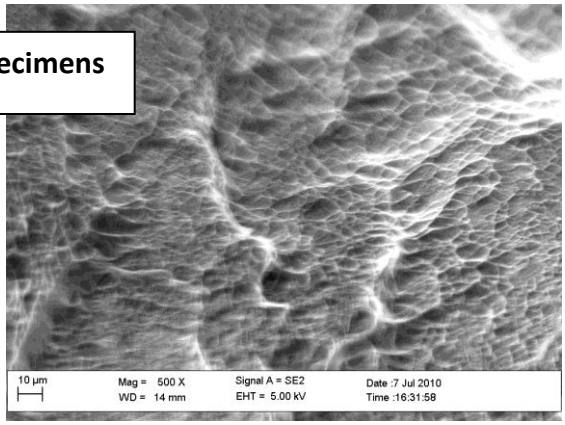

Figure 34: Fracture surface of the horizontal specimen after tensile testing

The horizontal specimen shows striations in the fracture surface consistent with ductile failure, however it also shows micro-voids that suggest brittle failure. This is consistent with the values obtained by mechanical testing, as the horizontal specimens had improved tensile strength and elongation compared to the vertical specimens but lower properties than the rolled plate (see Figure 30). This reduction in mechanical properties may be partly due to the porosity of the specimen as seen in Figure 37.

Vertical Specimens

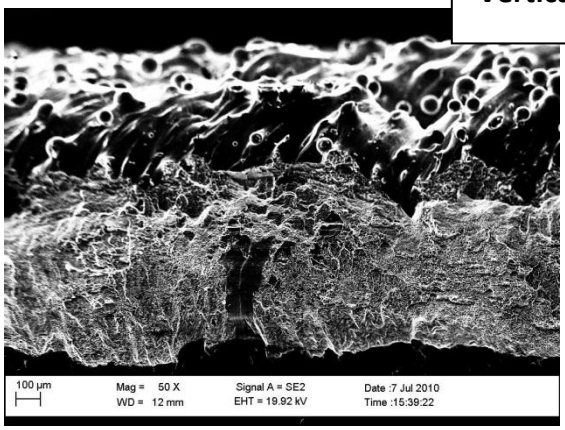

Figure 35: Fracture surface of the vertical specimen after tensile testing

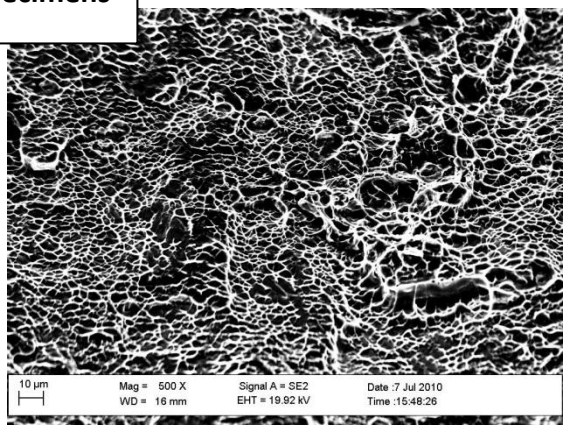

Figure 36: Fracture surface of the vertical specimen after tensile testing

The vertical specimen shows less void coalescence than the horizontal specimen, which suggests brittle failure. This specimen had the lowest tensile strength of those tested, which may be due to the surface finish as shown in Figure 37 (b). Sharp cracks at the surface act as stress concentrators and initiate brittle failure through the part, which would explain the low tensile strength and ductility of these specimens.

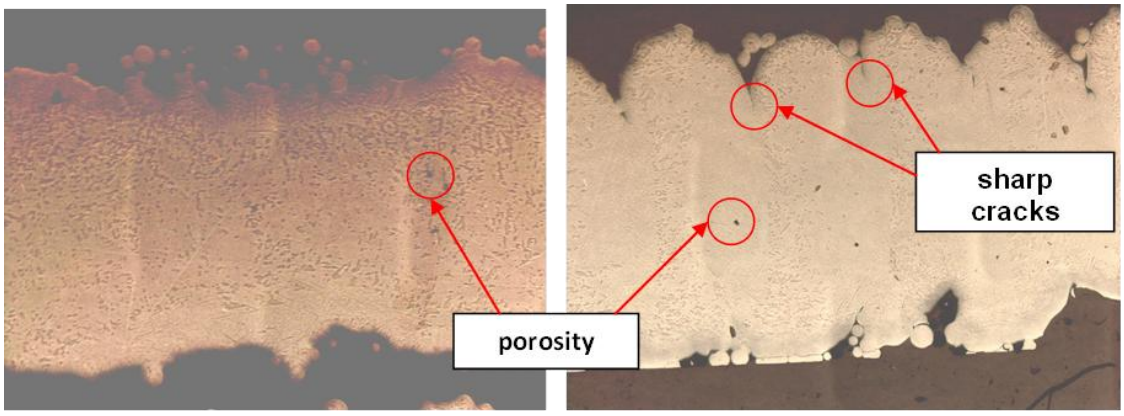

(a) (b)

Figure 37: Cross section of specimen cut in the (a) horizontal and (b) vertical direction

Figure 38 shows the cross section of a specimen machined out parts built in the x and z directions respectively, as seen using an optical microscope. A small amount of porosity is visible in both samples. In the vertical specimen the layers are clearly visible and sharp cracks mark each layer. In tensile testing these sharp cracks will act as failure initiation sites and reduce the tensile strength and ductility of the vertical specimens.

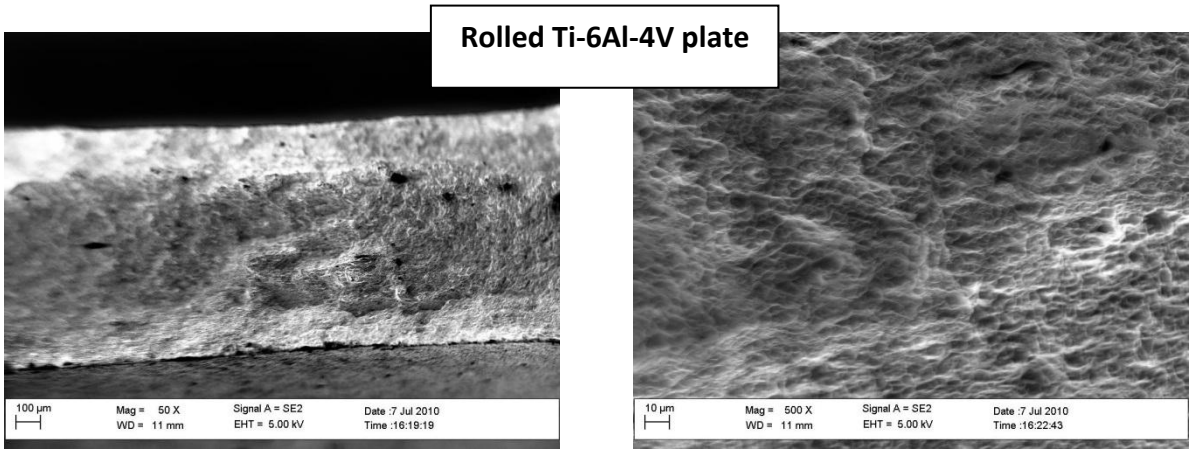

Figure 38: Fracture surface of the rolled Ti-6Al-4V plate after tensile testing

The rolled plate shows the elongation and the 'cup and cone' fracture surface typical of ductile failure. The mechanical properties of the plate compared to the standard data show that its performance is roughly within expected values, although only a small number of plate specimens were tested. However, this validates the testing carried out as it shows that it was possible to produce known values using this method.

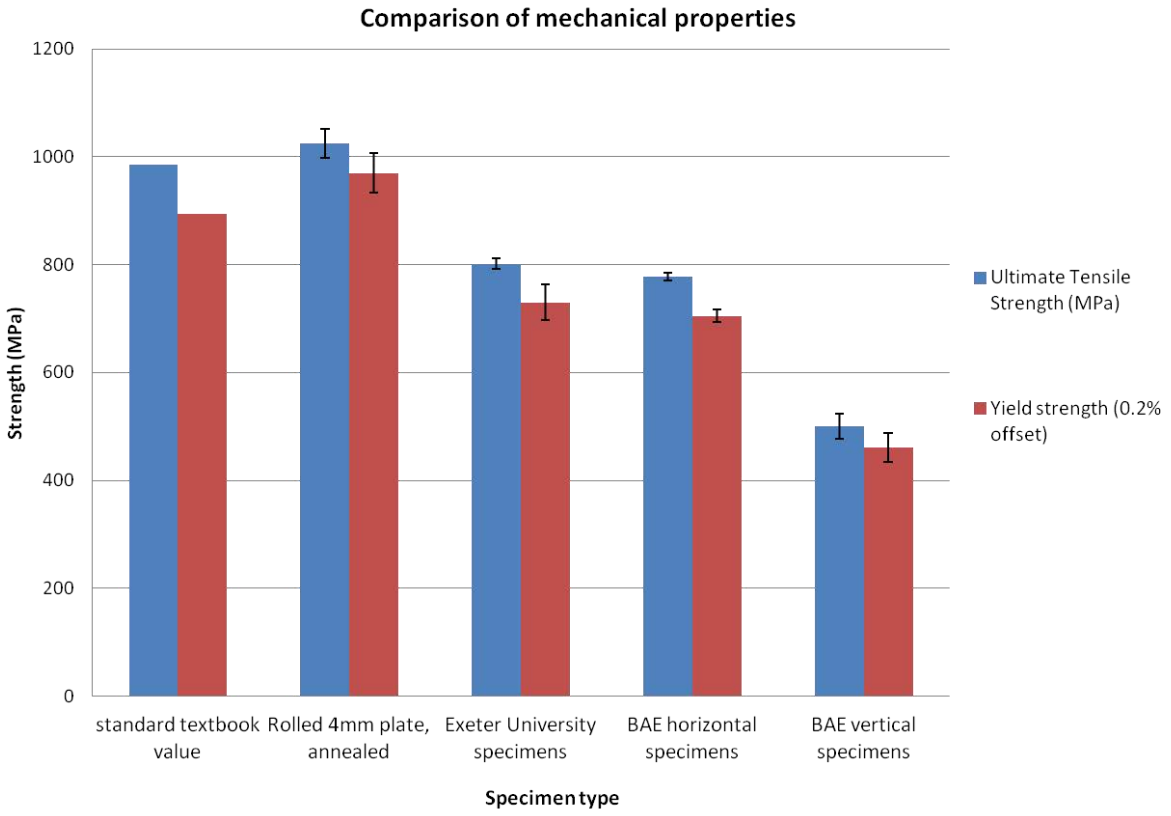

Figure 39: Comparison of tensile testing data from specimens built at BAE Systems, Exeter University, commercially manufactured rolled 4mm plate and standard textbook values [4]

As well the samples built using the DLD processing equipment at BAE system, the TSB project also involved the comparison of samples made at Exeter University and samples cut from rolled plate. These specimens were all mechanically tested to destruction using the same testing rig and all results were plotted as show in Figure 39, with standard textbook values for Ti-6Al-4V plotted for comparison. The DLD process used at Exeter University does not have directional bias and the results of mechanical testing show that the strength of parts produced there is comparable to parts made at BAE systems when cut in the horizontal direction with respect to build direction. The fact that the strength of the same specimens

when cut in the vertical direction is shown to be much lower supports the assumption that the sharp cracks that result from the layering will lead to brittle rather than ductile failure.

4.3.3 Comparison of microstructures developed under different thermal conditions

The general microstructure developed during each repair is seen in Figure 40, which shows micrographs of a central section of each repair.

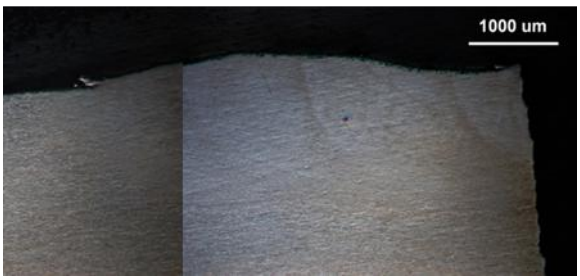

Plate 1 – heated (200°C)

Plate 2 – unclamped

Plate 3 – insulated

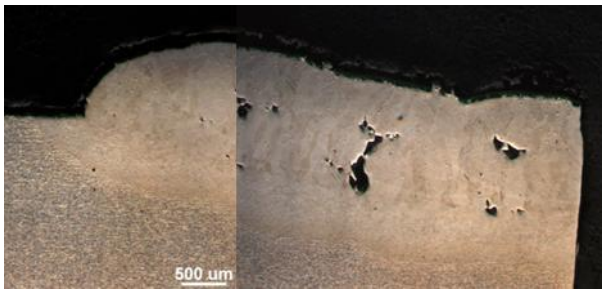

Plate 4 – cooled (10°C)

Plate 5 – clamped

Figure 40**:** Microstructures developed under different thermal conditions

Smallest HAZ **Largest HAZ**

Plate 4	Plate 2	Plate 5	Plate 3	Plate 1
cooled	unclamped	clamped	insulated	heated

The heat affected zone (HAZ) is the area of parent material that has been altered by the heat of processing. The HAZ is generally a weak point in a repair as the material properties are not as good as that of the parent material or repair material. By controlling the depth of the HAZ and keeping it small, the quality of the repair can be improved. The HAZ was measured from the micrographs and it was seen that the size of the HAZ increased as the temperature of the substrate was increased.

Highest porosity **Lowest porosity**

Plate 4	Plate 5	Plate 2	Plate 3	Plate 1
cooled	clamped	unclamped	insulated	heated

The porosity of the repair is a good indicator of its strength. The plate which underwent forced cooling to 10°C shows the highest porosity at all locations. This is because the surface does not get hot enough to form a good bond with the newly deposited layer of powder, so there is poor consolidation between layers. The adherence of the repaired material to the substrate is also poor.

The clamped plate (plate 5) had one edge free to move and so the right hand side distorted up and away from the work surface. The argon atmosphere essentially created an insulator between the plate and the work surface and so the right side of the plate becomes hotter

than the left. For this reason the size of the HAZ measured changes from cross sections across the plate, with the left hand side of the repair showing a deeper HAZ and higher porosity then the left hand side.

Plate 1 is preheated to 200°C so even the first layer of powder deposited is able to adhere fully to the substrate. When the plate is insulated it is initially at room temperature, but its temperature increases quickly as it is not able to dissipate into the work surface below. This means that although it shows very little porosity generally, the initial adherence to the substrate is not as good as that seen in the pre heated plate.

The unclamped plate distorted away from the work surface in both the longitudinal and transverse directions. Overall the average HAZ depth was greater than that of the clamped plate, although it was far more consistent across the plate.

The cooled plate consistently showed the poorest microstructure and the heated plate the best, with the insulated plate also showing constantly good properties. The insulated plate has the disadvantage of starting from room temperature, but otherwise the low thermal diffusivity of Ti-6Al-4V keeps the thermal gradient from becoming too steep. It also cools very slowly, leading to good consolidation between the layers.

4.4 Distortion measurements

The laser scanning before and after DLD processing was used to create the distortion maps shown in Figure 41.

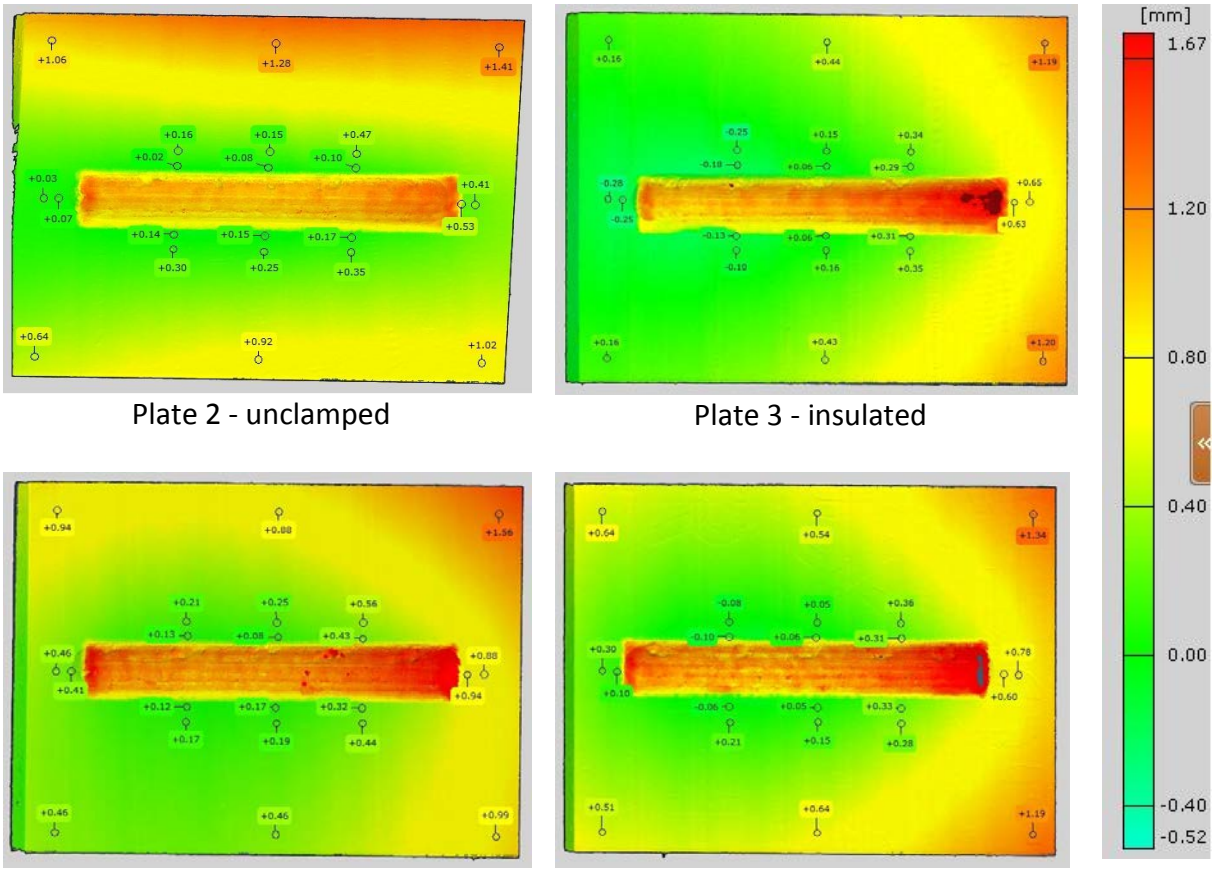

Plate 2 - unclamped

Plate 3 - insulated

Plate 4 – cooled (10°C)

Plate 5 - clamped

Figure 41 – overlaid scanning images showing changes in geometry after processing

The original scan for plate 1 (heated) unfortunately failed and so a distortion scan could not be produced. However, observation showed that the plate was distorted to approximately the same shape and magnitude as plate 3 (insulated).

All the plates show distortion towards the right hand side, which was the side unclamped to allow freedom. Only the completely unclamped plate shows significant distortion in the

longitudinal direction but it shows generally less distortion than the other plates. This is in agreement with the literature, which demonstrates that substrates which are clamped more tightly tend to show more distortion after processing [58]. For this reason distortion has been measured considering the centreline to be both horizontal (Figure 42) and vertical (Figure 43).

The distortion curves were obtained by measuring the distance from both the horizontal and vertical centreline of the plate to each thermcouple location. Distortion at each location was recorded by overlaying the distortion scans as shown in Figure 41, with the thermocouple holes giving precise refernece points. Thedistortion was plotted againts the distance from thr plate centreline in order to create the distortion curves.

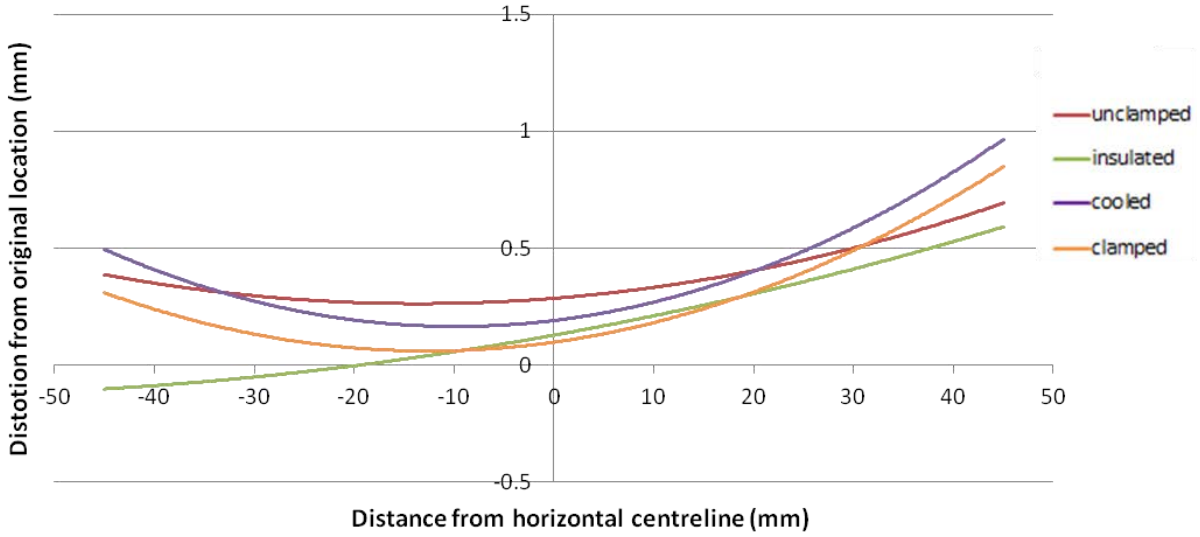

Figure 42: Distortion of Ti-6Al-4V plates processed at different thermal conditions away from the horizontal centreline

It is immediately clear that the distortion is not symmetrical about the centre of the plates. The asymmetrical clamping arrangement which was necessitated by the thermocouple positioning has had a significant effect on the distortion of the plates.

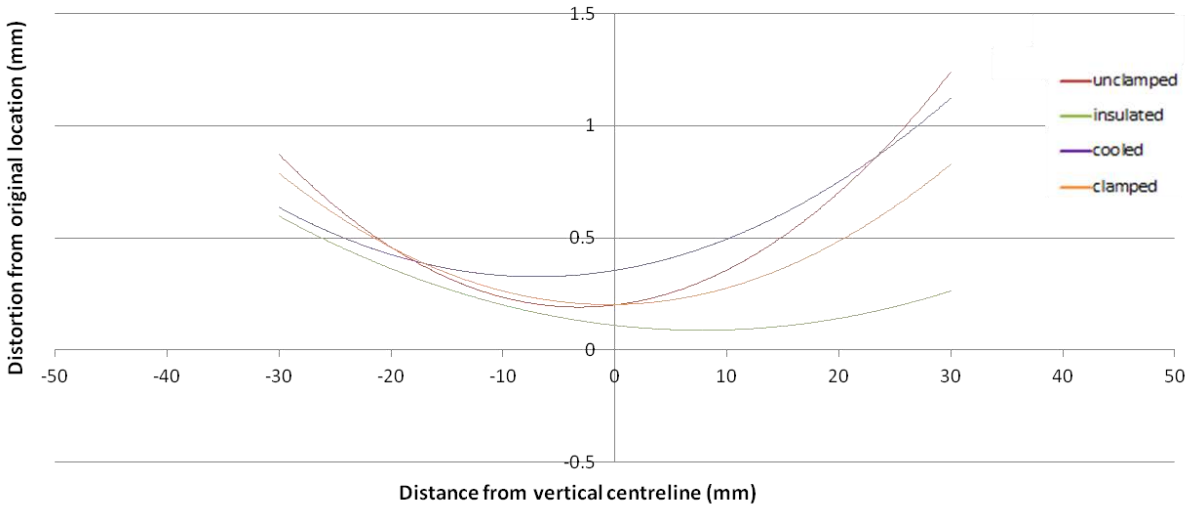

Figure 43: Distortion of Ti-6Al-4V plates processed at different thermal conditions away from the vertical centreline

The distortion is shown to be roughly symmetrical when measured against the horizontal centreline, with the exception of the insulated plate. There is also a greater difference between maximum and minimum distortion in this direction. In the horizontal direction the distortion is shown to be greater on the right hand side of the plate which had freedom to move.

Highest maximum distortion **Lowest maximum distortion**

Plate 4 cooled	**Plate 2 unclamped**	**Plate 5 clamped**	**Plate 3 insulated**

Again the insulated plate does not follow the trend of the other plates, suggesting it had not been evenly clamped to the work surface and was therefore not receiving equal insulation across the plate. Overall it shows the least distortion of all the plates, which corresponds with the theory that keeping the entire plate at a constant temperature can be used to reduce distortion.

4.5 Thermal gradients

The highly focussed laser heating used in DLD induces steep thermal gradients across the substrate. This effect is exacerbated by the low thermal diffusivity of Ti-6Al-4V, meaning that heat introduced to the substrate by the laser does not easily diffuse through the plate volume. The substrate area within the diameter of the laser beam becomes hot enough to be molten but in an unheated environment the edges of the plate will simultaneously be at room temperature. The difference in the temperature of the molten metal and cool edges is the thermal gradient, and the greater this difference is, the steeper the thermal gradient within the substrate.

Reducing the thermal gradient induced by DLD is expected to correspondingly reduce distortion induced by the process. The thermal conditions have been manipulated in each of the trials carried out.

Identifying the point at which the laser was switched on can be done using the readings from both the thermocouples and the thermal imaging camera (see appendix v). This means that the two data sets can be aligned and then the temperature reading given by each can be compared over time in order to determine if the calibration relationship is independent from temperature.

The thermocouples inserted into the plates took a temperature measurement sixty times a second. These values were plotted so that the change in temperature at various locations could be compared when processing took place under different thermal conditions (see Figure 48).

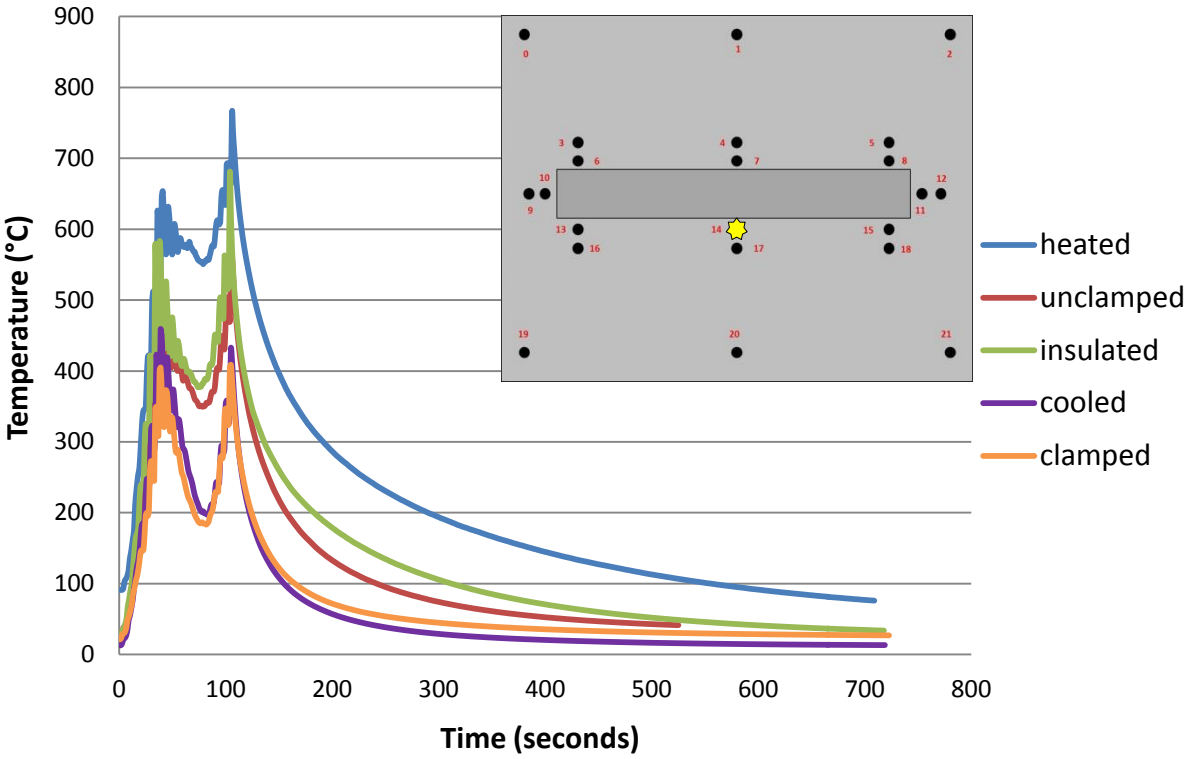

Figure 44: Temperature change over time at thermocouple location 14

In Figure 44 the temperatures recorded at location 14 (highlighted above) are compared. The peaks indicate the highest temperature reached at 105 seconds and the curve from this point shows the cooling rate from this peak temperature. It is this peak temperature and cooling rate that have the greatest effect on the developed microstructure, which agrees with the previous experience of other researchers as discussed in the literature review [4, 22, 41].

Location 14 is typical of the data measured by the thermocouples with respect to which plates display the highest peak temperatures and steepest cooling rate curves.

The cooling rate at each was taken to be the average for the first 100 seconds of cooling as this covers more than 75% of temperature loss in all locations. The data for all locations is included in the appendix.

Location	Distance from DLD area (mm)	Average cooling rate (°C/s) from peak temperature				
		Plate 1-heated (200°C)	Plate 2-unclamped	Plate 3-insulated	Plate 4-cooled (10°C)	Plate 5-clamped
0	30	0.5536	0.5656	0.2108	0.2178	0.2828
1	30	0.5468	0.767	0.4563	0.2161	0.4208
2	30	0.5366	0.6038	0.3964	0.4154	0.4154
3	5	3.6565	4.8684	2.0915	2.5138	5.3183
4	5	2.3544	4.55753	2.2878	2.5775	2.6075
5	5	2.1659	2.8882	2.6483	2.9885	3.2964
6	2	3.3666	3.1775	3.4728	5.0215	3.2
7	2	3.863	3.14	3.4986	4.6072	2.7788
8	2	1.8642	1.9934	1.9154	3.2256	2.0113
9	5	1.6919	1.7862	1.4114	1.6306	2.0842
10	2	1.6919	2.2691	1.88	1.6306	2.8546
11	-2	2.8703	3.1021	2.9115	3.2069	2.622
12	-5	2.0098	2.9007	2.1395	2.0836	1.9014
13	-2	4.7666	4.7458	4.9661	3.6412	3.0818
14	-2	4.8597	4.3491	5.0437	3.765	1.1516
15	-2	4.3994	4.4644	4.9993	4.2248	3.8091
16	-5	3.5963	3.4335	3.051	2.4458	2.0826
17	-5	3.609	3.2409	3.2619	2.6054	2.3551
18	-5	3.2339	3.164	3.4523	2.9705	2.8005
19	-30	0.4893	0.5791	0.1668	0.2517	0.2123
20	-30	0.7599	0.7217	0.4367	0.4215	0.4145
21	-30	0.6372	0.5713	0.4112	0.4225	0.3789

Table 6: Cooling rate at thermocouple locations across five experimental plates during the first 100 seconds after processing ended

Figures 45 and 46 show the rate of temperature change in different location, compared by plate.

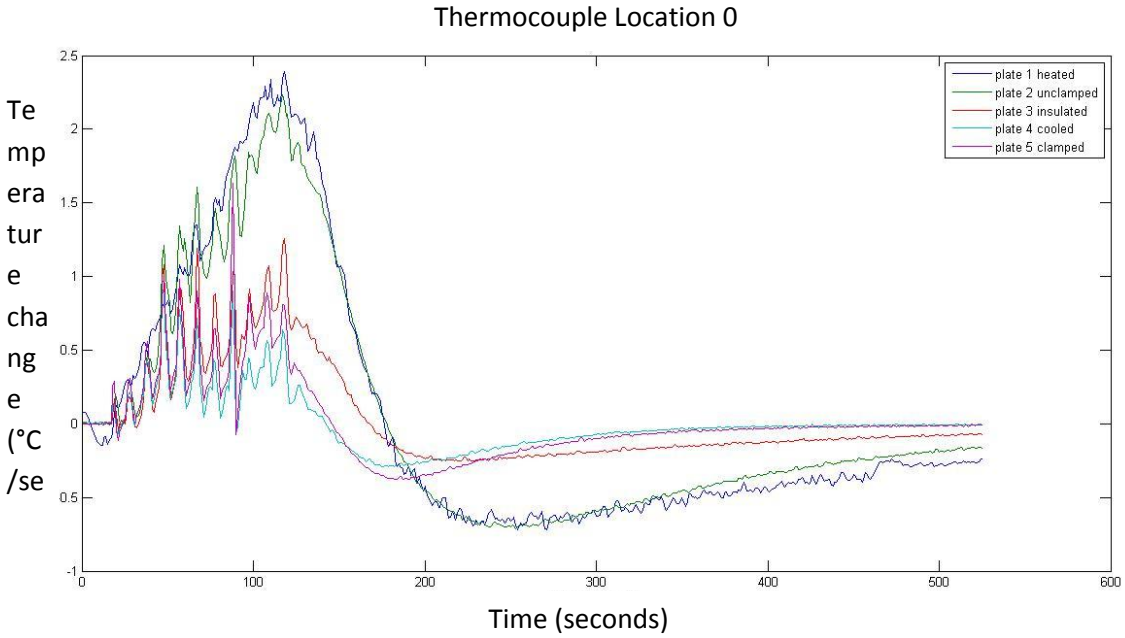

Figure 45: Temperature change (°C/s) during processing at thermocouple location 0

At location 0 the thermocouple is a long way from the laser heat source and so the effect of the applied thermal condition is greater than at location 15, which is very close to the processing. At location 0 the temperature change at the end of processing is much greater for the heated and unclamped plates and the gradient is the shallowest for the cooled plate. This indicates that cooling rate is much faster for the heated and unclamped plates than for the cooled plate at the edges of the substrate.

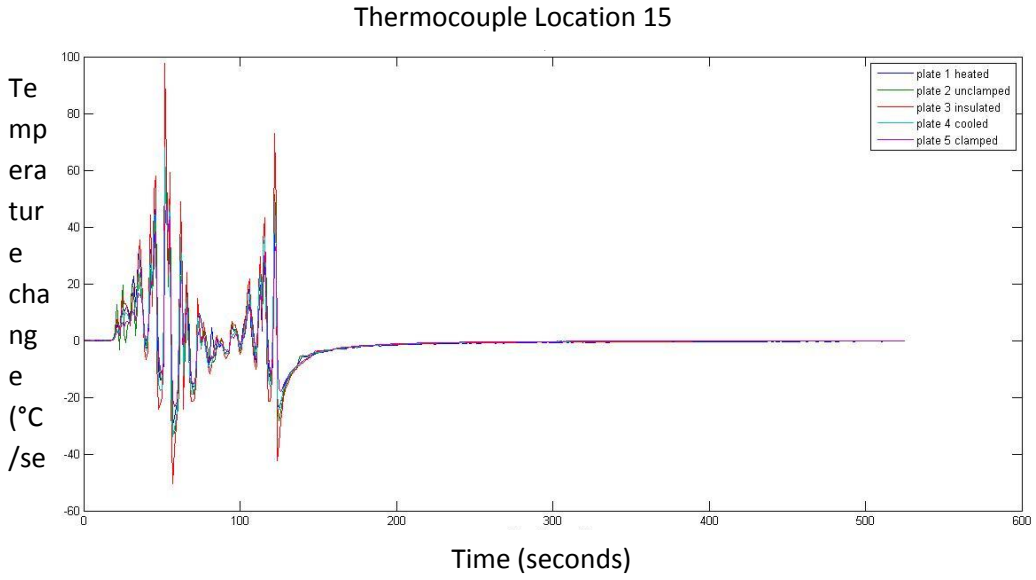

Figure 46: Temperature change (°C/s) during processing at thermocouple location 15

At location 15 there is far less difference in the temperatures and temperature change rate shown on each plate because the applied thermal conditions are no longer driving the peak temperature. Although the heated and unclamped plates reach higher peak temperatures, the cooling rate experienced by each plate at this location close to the processing area will be reasonably similar, with all plates returning to steady state very quickly after processing ends.

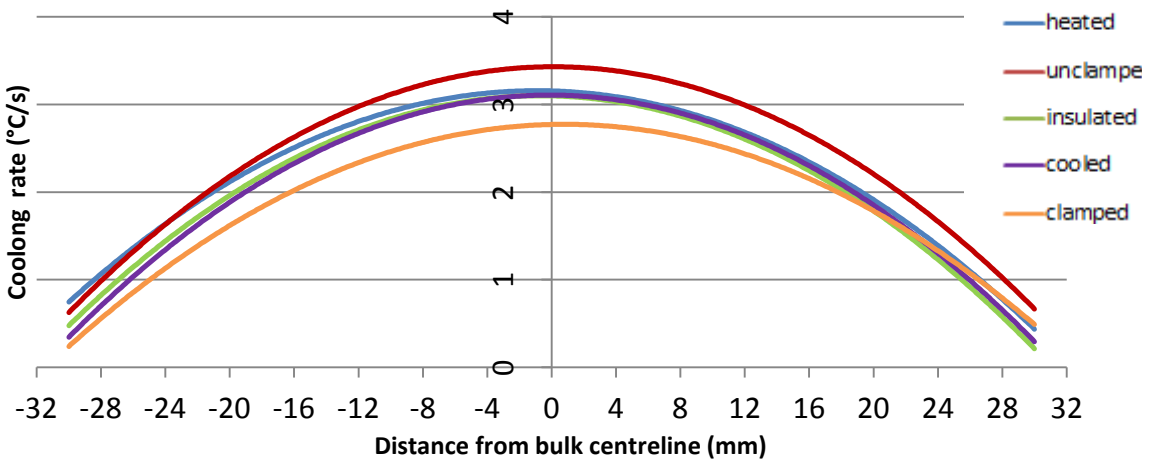

Figure 47: Trend of changing cooling rates with distance from the centreline of the plate

When plotted against distance, the cooling experienced by each plate follows roughly the same pattern, with every plate showing a decrease in cooling rate away from the centreline and processing area (see Figure 47).

The steepest cooling rate changes across the plate are in the unclamped plate. This is because it has distorted in both the longitudinal and transverse direction, making the contact between the plate and work surface very poor and allowing a greater build-up of thermal energy in the processed area that could not be conducted away.

Although the heated plate experienced the highest temperatures, the pre-heating was evenly applied and so the thermal; gradient is actually reduced by achieving a higher temperature at the outer edges of the plate. However the temperature is still increased in the processing area due to the low thermal diffusivity of the material.

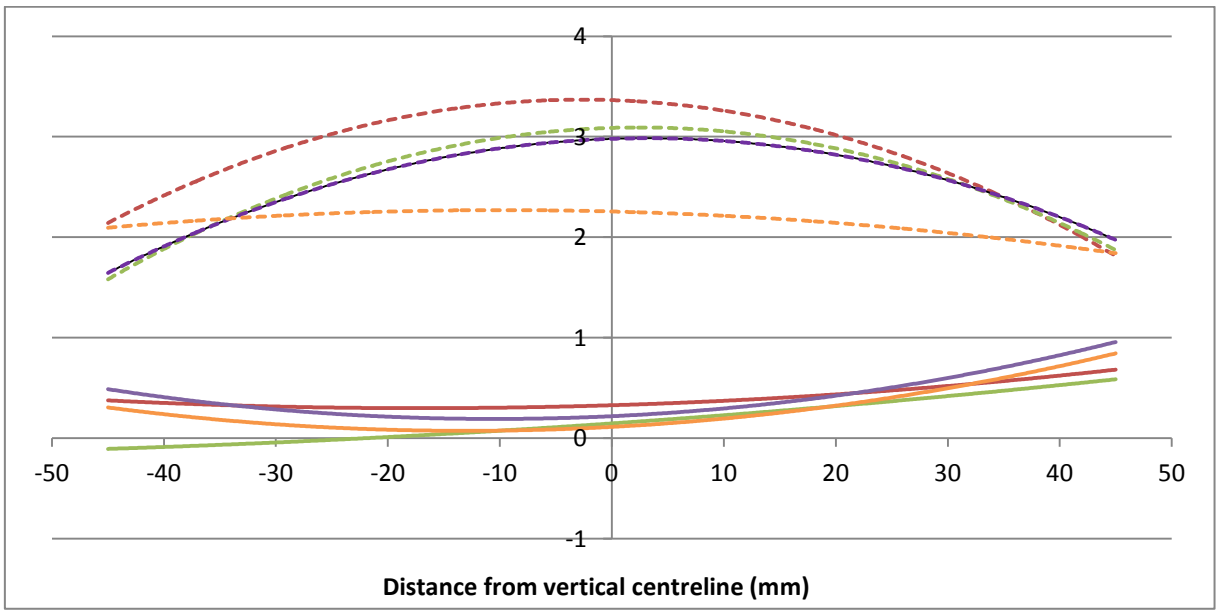

Figure 76: Cooling rate and distortion of Ti-6Al-4V plates

Plotting the cooling rate and distortion (see Figure 48) shows that the relationship between the two will be in the form of an inverse binomial equation;

$$.y = -mx^2 + bx + c \qquad \text{Equation 16}$$

4.6 Summary of results

The results discussed in this chapter can be considered to relate to either parameter optimisation, comparison of thin walled primary structures built using different equipment or thermal management of the DLD process for repair. The objectives of the project were to understand the influence of thermal boundary conditions, and to develop an understanding of the relationship between cooling rate and distortion. The results gathered can be used to advance knowledge of the DLD process for industrial use.

5 Conclusions

The aim of this project was to assess the influence of thermal boundary conditions on thermal cycles, microstructure and distortion of Ti-6Al-4V repairs performed by DLD. This was in order to develop an understanding of the relationship between cooling rate and distortion. The following conclusions have been reached based on the results gathered from the experimental work combined with the literature survey.

5.1 Influence of thermal conditions

- The porosity of repair material and the size of the heat affected zone improve inversely to one another with regard to the thermal conditions. This is not because a small heat affected zone causes low porosity or vice versa, it is because in the case of Ti-6Al-4V the same processing conditions are needed to produce both effects. Constant steady heating and fast cooling lead to the good consolidation necessary for low porosity also create a small heat affected zone after processing [10].
- The largest thermal gradient across the entire plate is in the cooled plate as it is having heat applied in the centre and extracted everywhere else. This means that the rate of change of temperature was the fastest in this plate and also that the distortion was very pronounced. The only plate which showed greater distortion was the clamped plate, which agrees with the theory that clamping during DLD introduces residual stresses leading to increased distortion [59].
- Cooling rates vary greatly at outer edges but hardly at all near the processing area. Therefore while the thermal gradient across the plate will affect distortion it will have little effect on microstructure.

- It had previously been assumed that the argon atmosphere in the processing chamber would act like an insulator, but the higher cooling rate on the right hand side of the plates (where they were free to distort away from the work surface) suggest that the gas being blown into the environmental chamber is actually a more efficient means of removing heat from the plate than conduction to the steel work surface below.
- The cooled plate has significant distortion, but the clamped plate has the highest distortion and the insulated plate in general has the lowest distortion (although there are some anomalies). This agrees with the theory that distortion is maximised by creating steep thermal gradients and by clamping during processing [51,59], suggesting that the next step for reducing distortion is to use insulation and/or preheating to try and maintain a constant temperature during processing. It may also be possible to use preheating to mitigate the effects of clamping on stress induction.

5.2 Relationship between cooling rate and distortion

- Plotting distortion against cooling rate shows there is an inverse relationship of the form of an inverse binomial equation. There are many assumptions made here and only a small amount of data has been used, so this should be taken more as a guide to the form of the relationship rather than quantitative evidence. It does however validate the experiments carried out as the results of the distortion and cooling rate measurements are found to agree with well-established theories.

5.3 Summary

The objectives of the project were to understand the influence of thermal boundary conditions, and to develop an understanding of the relationship between cooling rate and distortion. The conclusions that have been drawn from the results gathered provide more information about the effect of controlling thermal conditions on the outcome of the DLD process and also gives a guide to the form of relationship that is seen between cooling rate and distortion. These are both useful conclusions which represent an increase in knowledge in the subject area.

6 Future work

There are many areas in this project that could benefit from further study. The number of samples considered was very small and the conclusions reached would stronger if they were successfully repeated. It would also have been very useful to conduct tensile testing and hardness testing of the samples produced in order to get more information about the quality of the repairs to compare with parent material. This is important because it is the in-service performance or components repaired using DLD that will decide if it becomes a commonly used technique.

The direction of further research in this area will always be driven by industrial requirements and so the various extensions to the project have been grouped as for practical applications.

- Improved microstructure

This project has shown that a better consolidated and even microstructure can be achieved by applying or retaining heat, so that the rate of temperature change is reduced. Further useful study could undertake to find the optimum peak temperature for a Ti-6Al-4V plate to be maintained at and to investigate if microstructure could be further improved by further slowing the cooling rate.

- Improved design capabilities

In order to extend this research for use in genuine aerospace manufacture and repair, it would need to deal with geometries much larger and potentially asymmetric in shape. Current studies are investigating the effect of using DLD technology on large scale components, but it would also be useful to extend the knowledge of how heat is transferred in a component undergoing DLD when it cannot be said to be equally heated or insulated.

The failure of this project to keep plates clamped symmetrically has highlighted that this is an avenue worthy of investigation.

- Improved mobility

For DLD to be considered as a truly useful repair technique it would need to be not just reliable and adaptable to different geometries, but also portable. Now the understanding of what the process itself must accomplish to achieve good results is better understood, the equipment could start to be examined with regards to making it mobile. There are a number of challenges this would present, not least the need for an inert atmosphere, but having the ability to carry out DLD field repairs would significantly reduce the lead time needed to repair damaged components.

- Reduced costs

A major step in reducing the cost of DLD will be producing numerical and analytical models that will reduce the need for physical prototyping. A finite element model which described the geometry of the substrate, the boundary conditions and the laser heat source could be verified using experimental data and then use to predict the cooling rates and distortion experienced by different parts.

Microstructural maps are a way of describing the changes in the microstructure of a specimen as the distance from the point of heating increases. When studying the specimens cut from the experimental plates in this project the depth of the HAZ in both x and y direction was measured as well as changes in the size of the grains and the distribution of alpha and beta grains. Other features such as porosity have also been noted. Combining this information with accurate modelling of the thermal cycle caused by DLD will help to produce predictive microstructural maps. These maps can be compared to see how the

microstructural development has varied between plates and at different locations in the same place. It may also be possible to use preheating to mitigate the effects of clamping on stress induction

Some work has already been done in producing predictive model and microstructural maps for similar processes as discussed in the literature review and the consideration of modelling processes that accompanied this project is included in the appendix.

- Environmental concerns

At present, environmental and economic concerns are strong drivers in the development of new technologies. DLD makes good and economical use of expensive materials such as titanium but as yet there is no standard practice for recycling the waste powder that ensures it is still of the same high standard. It is also worth further investigating if insulation could be used in place of preheating to achieve constant temperatures as this would reduce the energy burden of creating parts using direct laser deposition.

References

1. **Richter, K., Behr, W. and Reisgen, U**. Low Heat Welding of Titanium Materials with a Pulsed Nd:YAG Laser (2007) Wiley Online Library
2. **Qian, L.** The influence of direct laser deposition variables on the microstructure of Ti-6A-4V (2006) PhD thesis University of Birmingham
3. **Gasser, A., Wissenback, K., Kelbassa, I., & Backes, G.** Laser Cladding: Aero engine repair-Laser metal deposition as a repair technique for high-value aero engine components.(2007) Industrial Laser Solutions for Manufacturing vol. 22 p15-21
4. **Lutjering, G. and Williams, J.C**. Titanium – 2nd edition (2007) Springer-Verlag
5. eFunda Titanium alloys – general information, available from http://www.efunda.com/materials/alloys/titanium/titanium.cfm
6. **Smith, W.** Structure and Properties of Engineering Alloys – 2nd edition (1993) McGraw-Hill
7. **Duley, W.** CO2 lasers, effects and applications (1976) London Academic Press p1-2
8. **Boyd, I.W.** Laser processing of thin film and microstructures: oxidation, deposition and etching of insulators (1987) Springer-Verlag p7-10
9. **Steen, W.M.** Laser material processing 1991 London Springer-Verlag London Limited p7-14
10. **Atwood, C. Griffith, M. Harwell, L. , Schlienger, E.,Ensz, M., Smueresky, J., Romero, T., Greene, D. and Reckaway, D** Laser Engineered Net Shaping (LENS™): A tool for direct deposition of metal parts (1998) Sandia National Laboratories, Albuquerque, US Department of Energy

11. **Motyka, M., Kubiak, K., Sieniawski J. and Ziaja, W**. Hot Plasticity of Alpha Beta Alloys, Titanium Alloys - Towards Achieving Enhanced Properties for Diversified Applications (2012) InTech, available from: http://www.intechopen.com/books/titaniumalloys-towards-achieving-enhanced-properties-for-diversified-applications/influence-of-processing-conditionson-hot-plasticity-of-alfa-beta-titanium-alloys
12. eFunda Highlights of Selective Laser Sintering, available from http://www.efunda.com/processes/rapid_prototyping/sls.cfm?search_string=sls#PageTop
13. **Ahmed, T. and Rack, H.J.** Phase transformations during cooling in α+β titanium alloys (1998) Materials Science and Engineering vol. A243 p206-211
14. **Laeng, J. Stewart J.G. and Liou F.W.** Laser metal forming processes for rapid prototyping – a review (2000) International Journal of Production Research vol. 38 p3973-3996
15. **Seefeld, T. Theiler, C. and Sepold, G.** Increasing the process efficiency in laser beam cladding 2002 p158-163 International Conference on Metal Powder Deposition for Rapid Manufacturing San Antonio, Texas
16. **Toyserkani, E. Khajepour, A. and Corbin, S.** Laser cladding (2005) CRC Press LLC
17. **Hu, D. and Kovacevic, R.** Sensing, modelling and control for laser-based additive manufacturing (2003) Journal of Machine Tools and Manufacture vol. 43 p51-60
18. **Hofmeister, W. and Wert, M.** Investigating solidification with the laser engineered net shaping process (1999) Journal of Materials vol. 51 p1-6
19. **Majumder, J.D., Pinkerton, A., Liu, Z., Manna, I. and Li, L**. Microstructure characterisation and process optimisation of laser assisted rapid deposition of 316L stainless steel (2005) Applied Surface Science vol. 247 p320-327

20. **Wu, X., Sharman, R., Mei, J. and Voice, W**. Microstructure and properties of a laser fabricated burn-resistant Ti-alloy (2003) Materials & Design vol. 25 p103-109
21. **Wu, X. and Mei, J.** Near net shape manufacturing of components using direct laser deposition technology (2003) Journal of Materials Processing Technology vol. 135 p266-270
22. **Wu, X., Liang, J., Mei, J., Mitchell, C., Goodwin, P.S. and Voice, W** Microstructures of laser deposited Ti-6Al-4V (2004) Materials & Design vol. 25 p137-144
23. **Kobryn, P.A., Moore, E.H. and Semiatin, S.L.** The effect of laser power and traverse speed on microstructure, porosity and build height in laser-deposited Ti-6Al-4V (2000) Scripta Material vol. 43 p299-305
24. **Kelly, S.M., Kampe, S.L. and Crowe, C.R.** Microstructure Study of Laser formed Ti-6Al-4V (2000) Proceedings, Solid Freeform and Additive Fabrication – Materials Research Society Symposium, San Francisco
25. **Tiley, J., Searles, T., Lee, E., Kar, S., Banerjee, R., Russ, J.C. and Fraser, H.L**. Quantification of microstructural features in α/β titanium alloys (2004) Materials Science and Engineering vol. 372 p191-198
26. **Liu, C.M., Tian, X.J., Tang, H.B., and Wang, H.M.** Microstructural characterisation of laser-melting deposited Ti-5Al-5Mo-5V-1C-1Fe near-β titanium alloy (2013) Journal of Alloys and Compounds vol.572 p17-24
27. The Ultimate Infrared Handbook for R&D Professionals (2011) FLIR Systems AB http://www.flir.com/thg
28. **Griffith, M. and Schlienger, M.,** Understanding thermal behaviour in the LENS process (1999) Materials & Design vol. 20 p107-113

29. **Kelly, S.M. and Kampe, S.L.,** Characterisation and thermal model of laser formed Ti-6Al-4V (2002) Proceedings of International Conference on Metal Powder Deposition for Rapid Manufacturing p104-111
30. **Von Allmen, A. and Blatter, A**. Laser beam interactions with materials – physical properties and applications (1995) Springer-Verlag p41-43
31. **Prokhorov, A.M. and Konov, V**. Laser heating of materials (1990) IOP Publishing Ltd p40
32. **Rubahn, H.G.** Laser applications in surface science and technology (1999) John Wiley and Sons p186
33. **Grong, O**. Metallurgical Modelling of Welding – 2nd edition (1997) Materials Modelling Series, Institute of Materials
34. **Ward, R.M., Barrat, M.D., Jacobs, M.H., Zhang, Z. and Dowson, A.L.** A simple transient numerical model for heat transfer and shape evolution during the production of rings by centrifugal spray deposition (2004) Journal of Materials Science vol. 39 p7259-7267
35. **Qian, L., Mei, J., Liang, J. and Wu, X.** Influence of position and laser power on thermal history an microstructure of direct laser fabricated Ti-6Al-4V samples (2005) Materials Science and Technology vo. 21 p597-605
36. **Kelly, S.M. and Kampe, S.L**. Microstructural evolution in laser deposited multilayer Ti-6Al-4V builds: part I microstructural characterisation (2004) Metallurgical and materials transactions A – physical metallurgy and materials science vol. 35 p1861-1867
37. **Brandl, E., Michailov, V., Viehweger, B. and Leyens, C.** Deposition of Ti-6Al-4V using laser and wire, part 1: Microstructural properties of single beads (2011) Surface and Coatings Technology vol. 206 p1120-1129

38. **Shuangyin, Z., Xin, L., Jing, C., & Weidong, H**. Influence of heat treatment on the microstructure and properties of Ti-6Al-4V titanium alloy by laser rapid forming. (2007) Rare Metal Materials and Engineering vol. 36 p1263
39. **Wang, F., Mei, J., & Wu, X**. Microstructure study of direct laser fabricated Ti alloys using powder and wire (2006) Applied Surface Science, vol. 253 p1424-1430
40. **Baufeld and Van der Beest** Mechanical properties of Ti-6Al-4V specimens produced by shaped metal deposition (2009) IOP Publishing Science and Technology of Advanced Materials
41. **Kelly, S.M. and Kampe, S.L.** Microstructural evolution in laser deposited multilayer Ti-6Al-4V builds: part II thermal modelling (2004) Metallurgical and materials transactions A – physical metallurgy and materials science vol. 35 p1869-1879
42. **Charles, C.** Modelling microstructure evolution of weld deposited Ti-6Al-4V (2008) PhD thesis, Lulea University of Technology
43. **Masubuchi, K.** Residual Stresses and Distortion (1993) ASM Handbook vol. 6 Welding, Brazing and Soldering
44. **Das, S., Wohlert, M., Beaman, J.J. and Bourell, D.L.** Processing of titanium net shapes by SLS/HIP (1999) Materials and Design vol. 25 p114-121
45. **Tsay, L.** Fatigue crack growth behaviour of laser-processed 304 stainless steel in air and gaseous hydrogen (2003) Corrosion Science vol. 45 p1985-1997
46. **Giren, B.**G., The influence of residual stresses on cavitation resistance of metals – an analysis based on metal remelted by laser beam and optical discharge plasma (1999) Wear p86-92

47. **Dai, K.**, Thermal and stress modelling of multi-material layer processing (2001) Acta Mater. Vol. 49 p4171-4181
48. **Karaptis, N.** Thermal behaviour of parts made by direct metal laser sintering (1998) Solid Freeform Fabrication p79-88
49. **Dalgarno, K.**W. Finite element analysis of curl development in the selective laser sintering process (1996) Solid Freeform Fabrication proceedings p559-566
50. **Chin, R.** Successive deposition of metals in solid freeform fabrication processes, part 2; thermomechanical models of layers and droplet columns (2001) Journal of Manufacturing Science and Engineering vol. 123 p632-638
51. **Dai, K.** Thermal and mechanical finite element modelling of laser forming metal and ceramic powders (2003) Acta Mater vol. 52 p69-80
52. **Chin, R.**K. Thermomechanical modelling of molten metals droplet solidification applied to layered manufacturing (1996) Mechanics of Materials vol. 24 p 257-221
53. **Moraitis, G.A., and Labeas, G.N.** Prediction of residual stresses and distortions due to laser beam welding of butt joints in pressure vessels (2009) International Journal of Pressure Vessels and Piping vol. 86 p133-142
54. **Ghosh, S.** Three-dimensional transient finite element thermal stress analysis for laser aided DMD process (2003) International Congress on Applications of lasers and electro-optics (ICALEO) Jacksonville, Florida p1308-1320
55. **Wang, L., Felicelli, S., Gooroochurn, Y., Wang, P.T. and Horstemeyer, M.F.** Optimization of the LENS process for steady state molten pool size (2008) Materials Science and Engineering vol. 474 p148-156

56. **Ye, R., Smueresky, J.E., Zheng, B., Zhou, Y. and Lavernia, E.J.** Numerical modelling of the thermal behaviour during the LENS process(2006) Materials Science and Engineering vol. 428 p47-53
57. **Wang, L. and Felicelli, S**. Analysis of thermal phenomena in LENS deposition (2006) Materials Science and Engineering vol. 435-436 p625-631
58. **Klingbeil, N., Beuth, J., Chin, R.K. and Amon, C.H.** Residual stress-induced warping in direct metal solid freeform fabrication (2002) International Journal of Mechanical Sciences vol. 44 p57-77
59. **Nickel, A.H., Barnett, D.M. and Prinz, F.B.** Thermal stresses and deposition patterns in layered manufacturing (2001) Materials Science and Engineering vol. 317 p59-64
60. **Jendrzejewski, R. and Sliwinski, G**. Investigation of temperature and stress fields in laser cladded coatings (2007) Applied surface science p921-925
61. **Tolle, F., Gumenyuk, A., Backhaus, A., Rethmeier, M. and Reisgen, U.** *Welding residual stress reduction by scanning of a defocused beam* (2012) Journal of Materials Processing Technology vol. 212 p19-26
62. **ASTM Standard E8/E8M**, "Standard Test Methods for Tension Testing of Metallic Materials," ASTM International, West Conshohocken, PA, 2008, DOI: 10.1520/E0008_E0008M, www.astm.org
63. **Vasinonta, A., Beuth, J. and Griffith, M.** Process maps for controlling residua stress and melt pool size in aser based SFF process (2000) presented at Solid Freeform Fabrication Symposium